

AD-A238 521



DTIC

JUL 1991

2

## Semi-Annual Letter Report

**Growth, Nitrogen Vacancy Reduction and Solid Solution  
Formation in Cubic GaN Thin Films and the Subsequent  
Fabrication of Superlattice Structures Using AlN and InN**

Supported under Grant #N00014-86-K-0686 P5  
Innovative Science and Technology Office  
of the Strategic Defense Initiative  
Office of the Chief of Naval Research  
Report for the period January 1, 1991-June 30, 1991

Robert F. Davis, Michael J. Paisley and Zlatko Sitar  
Materials Science and Engineering Department  
North Carolina State University  
Campus Box 7907  
Raleigh, NC 27695-7907

June, 1991

Unclassified

91 7 18 008

91-05475



**Best  
Available  
Copy**

REPORT DOCUMENTATION PAGE			Form Approved OMB No 0704 0188	
<small>Public reporting burden for this collection of information is estimated to average 1 hour per response, including the time for reviewing instructions, searching existing data sources, gathering and maintaining the data needed, and completing and reviewing the collection of information. Send comments regarding this burden estimate or any aspect of this collection of information, including suggestions for reducing this burden, to Washington Headquarters Services, Directorate for Information Operations and Reports, 1215 Jefferson Davis Highway, Suite 1204, Arlington, VA 22202-4302, and to the Office of Management and Budget, Paperwork Reduction Project (0704-0188), Washington, DC 20503.</small>				
1. AGENCY USE ONLY (Leave blank)		2. REPORT DATE June, 1991		3. REPORT TYPE AND DATES COVERED Semi-Annual Letter 1/1/91-6/30/91
4. TITLE AND SUBTITLE Growth, Nitrogen Vacancy Reduction and Solid Solution Formation in Cubic GaN Thin Films and the Subsequent Fabrication of Superlattice Structures Using AlN and InN			5. FUNDING NUMBERS R&T:s400001srq05 S.O.:1114SS	
6. AUTHOR(S)  Robert F. Davis				
7. PERFORMING ORGANIZATION NAME(S) AND ADDRESS(ES)  North Carolina State University Hillsborough Street Raleigh, NC 27695			8. PERFORMING ORGANIZATION REPORT NUMBER  N00014-86-K-0686 P5	
9. SPONSORING/MONITORING AGENCY NAME(S) AND ADDRESS(ES) Sponsoring: ONR, 800 N. Quincy, Arlington, VA 22217 Monitoring: Office of Naval Research Resider, N66005 The Ohio State University Research Center 1314 Kinnear Road Columbus, OH 43212-1194			10. SPONSORING/MONITORING AGENCY REPORT NUMBER	
11. SUPPLEMENTARY NOTES				
12a. DISTRIBUTION/AVAILABILITY STATEMENT  Approved for Public Release; Distribution Unlimited			12b. DISTRIBUTION CODE	
13. ABSTRACT (Maximum 200 words)  An ALE deposition system, as well as our initial results of the ALE growth of GaN, are described. The deposition system was fabricated in-house. It is high vacuum capable and allows the introduction of up to 16 gases without mixing. The substrates travel under different zones, each of which allows the adsorption or decomposition of one gas species at a time. Continuous crystalline GaN films were grown on (0001) $\alpha$ -SiC and analyzed by Auger spectroscopy, scanning electron microscopy and electron diffraction. Research concerned with the heteroepitaxial deposition of cubic boron nitride (c-BN) using different substrates and deposition technologies has also been conducted. Films were deposited and analyzed using the techniques of reflection high energy electron diffraction (RHEED), x-ray photoelectron spectroscopy (XPS), low energy electron diffraction (LEED), x-ray diffraction (XRD), scanning electron microscopy (SEM), transmission electron microscopy (TEM), and Fourier transform infrared spectroscopy (FT-IR). The results of the deposition experiments and the subsequent analyses for both materials are discussed.				
14. SUBJECT TERMS gallium nitride, aluminum nitride, boron nitride, atomic layer epitaxy, layered structures, transmission electron microscopy, photoluminescence, gas-source MBE, laser ablation, borazine			15. NUMBER OF PAGES 42	
			16. PRICE CODE	
17. SECURITY CLASSIFICATION OF REPORT UNCLAS	18. SECURITY CLASSIFICATION OF THIS PAGE UNCLAS	19. SECURITY CLASSIFICATION OF ABSTRACT UNCLAS	20. LIMITATION OF ABSTRACT SAR	

## Table of Contents

<b>I. Atomic Layer Epitaxy of Gallium Nitride</b>	<b>1</b>
A. Introduction	1
B. Experimental Procedures	1
<i>Description of the III-V Nitride ALE System</i>	1
<i>Growth Theory</i>	7
<i>Growth and Analysis Procedures</i>	10
C. Experimental Results and Discussion	10
<i>Surface Morphology</i>	10
<i>Chemical Analysis</i>	12
<i>Electron Diffraction</i>	12
D. Conclusions	17
E. Future Research	17
<b>II. Growth of Cubic Boron Nitride</b>	<b>17</b>
A. Introduction	17
B. Selection of Substrate Materials, Deposition Technologies and Analytical Techniques	18
<i>Substrate Materials</i>	18
<i>Deposition Technologies</i>	18
<i>Analytical Techniques</i>	19
C. Experimental Procedures	20
<i>Gas Source MBE</i>	20
<i>Microwave Plasma CVD</i>	22
D. Results	24
<i>Gas Source MBE</i>	24
<i>Microwave Plasma CVD</i>	30
E. Discussion	33
<i>Gas Source MBE</i>	33
<i>Microwave Plasma CVD</i>	35
F. Conclusions	37
G. Future Research Plans/Goals	38
<i>Use of Copper Substrates</i>	38
<i>Lowered Growth Temperatures</i>	39
<i>Laser Ablation</i>	39
H. Acknowledgements	39
<b>III. References</b>	<b>39</b>

Approved For	
by	
DTIC ID	
Unclassified	
Justification	
by	
on	
Classification	
Excluded from	
Excluded from	
Excluded from	

A-1

# I. ATOMIC LAYER EPITAXY OF GALLIUM NITRIDE

## A. Introduction

At the present time, MBE and MOCVD are the two contenders for the growth of the most sophisticated semiconducting structures. Both can produce extremely thin layers and a wide range of compound semiconductors and heterostructures. However, in both techniques all the reactant species simultaneously arrive at the substrate. As such, there exist conditions for the growth of the next monolayer of the material before the growth of the previous one is even completed. As a result of that, the growth process becomes shared between several levels of monolayers. This occurs in practically all materials deposition systems and is easily observed at the study of the RHEED oscillations. One observes the damping of the oscillation amplitude with the film thickness. Because of that, the RHEED oscillations usually disappear after 10-20 monolayers of growth.

The ultimate technique, with the best control over the composition and the surface morphology, may be the deposition of a single layer, of one kind of atoms, at a time. This is done by Atomic Layer Epitaxy (ALE), a technique patented by Suntola and Atson in 1977 [1]. They used this method for the deposition of the polycrystalline ZnSe on the glass substrates and were primarily concerned with the thickness uniformity over the large areas. At the beginning, ALE seemed to work only for II-VI compounds. However, it was later shown that it works also for other materials. A comprehensive review of the ALE work on II-VI compounds has been published by Goodman and Pessa [2]. Much attention has been lately devoted to the ALE of GaAs. Several research groups have demonstrated the feasibility of the technique for III-V compounds [3,4].

Atomic Layer Epitaxy can be achieved with many present deposition techniques, and is the thought of as a special mode of operation of the known deposition techniques, rather than an entirely new deposition method. Since ALE growth consists of deposition cycles, in which a single monolayer of an individual species is deposited at a time, the final film thickness depends only on the number of cycles and the lattice parameter of the material. Thus ALE offers the ultimate control over the thickness and morphology of the layers, and has also the potential for the achievement of very good stoichiometry and the reduction of the point defects. Since the reactants are kept apart throughout the deposition, they are not subject to troublesome parasitic reactions in the gas phase.

## B. Experimental Procedures

*Description of the III-V Nitride ALE System.* To accomplish the ALE of III-V nitrides, a vacuum system has been designed and built, which allows the ALE deposition within the framework of MOCVD parameters. The system is configured to process 1 inch wafers.

Ultimately, the apparatus may be adapted to handle samples up to 2 inches in diameter. The system consists of three chambers; a load lock, a cleaning chamber, and a growth chamber, as shown in Figure 1. It is made of stainless steel parts with knife edge seals, and is high vacuum capable. Process gasses are regulated by mass flow controllers and pumped by a rotary vane pump. The ultimate vacuum is achieved by diffusion pumps.

The load lock is a simple five way cross that can hold up to five samples. All samples are introduced to and removed from the system through this chamber. By the present design, the load lock may be pumped down to the millitorr level.

After passing through the load lock, the samples are cleaned in the cleaning chamber by a remote argon plasma with the downstream injection of hydrogen. The cleaning chamber is pumped to high vacuum by a diffusion pump, while the process gases, used for cleaning, are handled by a rotary vane pump through an automatic throttle valve. To assure identical sample cleaning within a run, up to four samples can be cleaned at a time. This chamber is capable of performing many variations on the plasma cleaning operation, since it has capability of varying gas flow rates, substrate temperature, plasma intensity and process pressure.

After cleaning, the samples are transferred to the growth chamber. Like the cleaning chamber, the growth chamber is pumped to high vacuum conditions using a diffusion pump with an LN<sub>2</sub> trap, while the process gases are handled by a rotary vane pump. The process pressure is controlled by a combination of a capacitance pressure gauge and an automatic throttle valve. Inside the growth chamber, the samples sit on a revolving, heated, disk-like susceptor made of SiC coated graphite. The overall design allows heating up to 1000° C; however, the intention is to process at substantially lower temperatures. Due to the large mass and the possibility for the need for high deposition temperatures, appropriate heat shielding and water cooling have been installed.

A specially designed vane assembly allows the deposition in the ALE mode. The assembly is stationary above the rotating susceptor and consists of sixteen separate compartments for the introduction of up to sixteen (theoretically) different gases without mixing. As wafers travel under it, they see a different atmosphere under each zone. However, the ALE process requires a purge cycle with an inert gas after each exposure of the wafers to the reactants. This allows the time for the desorption of physisorbed molecules. After this cycle only the chemisorbed monolayer remains. If a purge is applied after every exposure to reactants, half of the zones (eight) remain for the deposition. That means, four zones for each reactant, when a binary compound is grown. This arrangement allows the growth of four monolayers (about 7-10 Å) of the binary compound per revolution of the susceptor. The anticipated growth rate in the ALE mode is about 1 µm per hour. Figure 2 shows the heart of the ALE system; i.e., the heater, the sample receiver and the vane assembly.

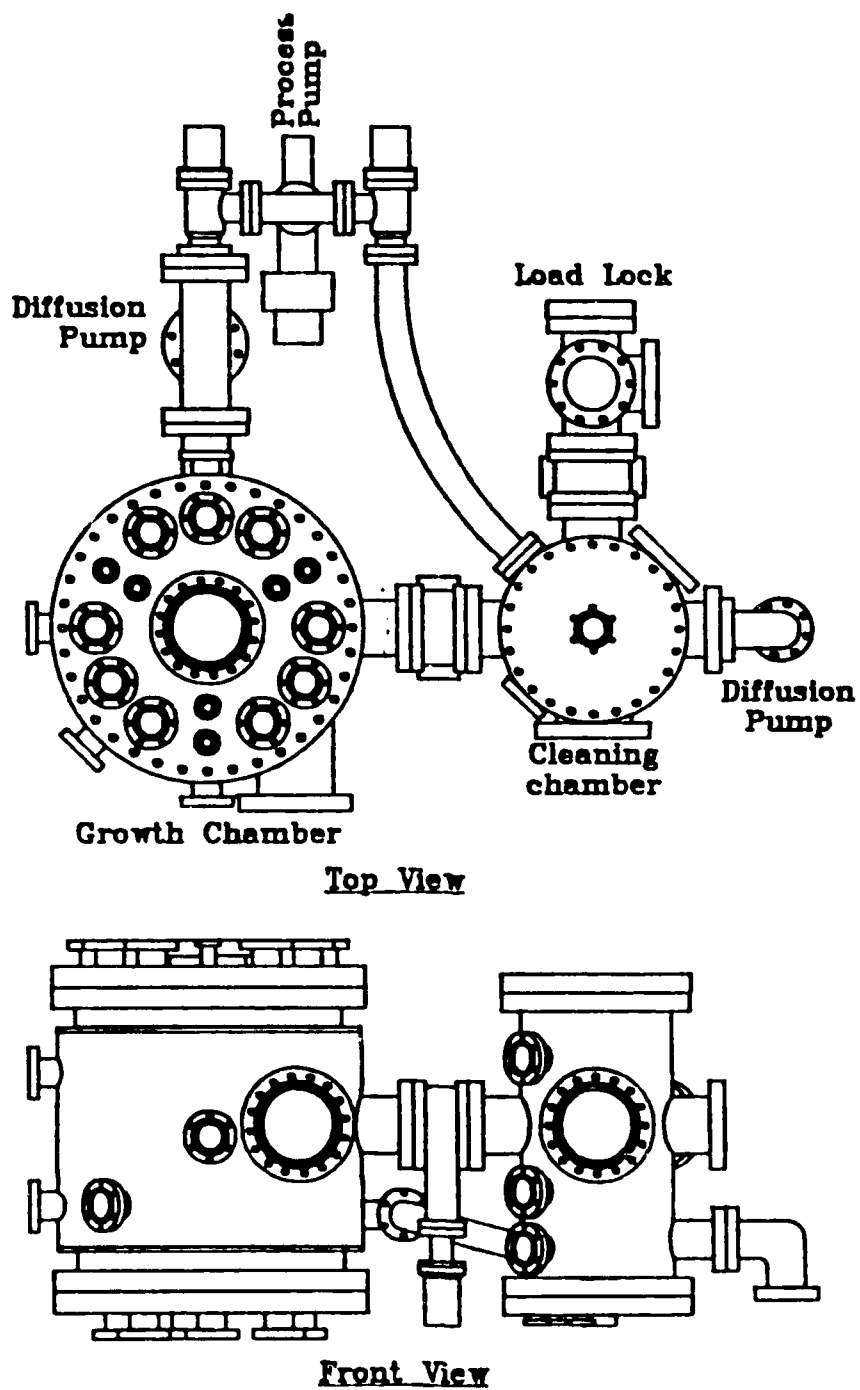


Figure 1. The top view of the ALE system showing all three chambers: load lock, cleaning chamber and growth chamber. The later two are visible also in the front view.

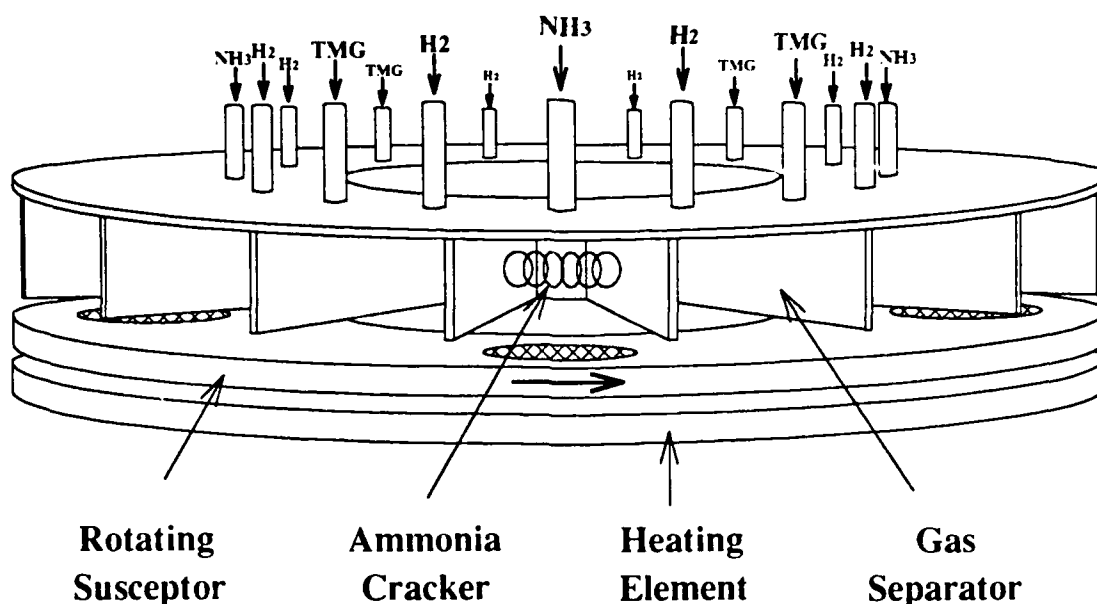


Figure 2. The heart of the ALE growth system: sample heater, rotating susceptor and the vane assembly. The vane assembly consists of sixteen separate compartments for the introduction of various gases without mixing.

Figure 3 shows a block diagram of the entire system, which can be divided into three parts: the vacuum chambers previously described, the gas introduction system, and the pumping system.

The gas introduction system is capable of handling organometallic (OM) and gaseous precursors. All gases used in the deposition are ultra high purity. They are further purified by chemical purifiers in each gas line. Each OM module consists of a bubbler sitting in a constant temperature bath, a capacitance pressure transducer for measuring the pressure inside the bubbler, a manual metering valve for the pressure control, a mass flow controller for the control of the flow rate of the carrier gas, and several manual and pneumatic shut-off valves.

All this hardware allows precise dosing of the OM into the reaction chamber via the control of three key parameters: bubbler temperature, bubbler pressure and the carrier gas flow rate. Since the partial pressure of the OM in the bubbler depends only on the temperature only, one can calculate the pressure (and therefore volume) ratio ( $X_{OM(T)}$ ), assuming ideal gas behavior, between the OM source and the carrier gas supplied into the reaction chamber simply as the ratio between the partial pressure of the OM at the bubbler



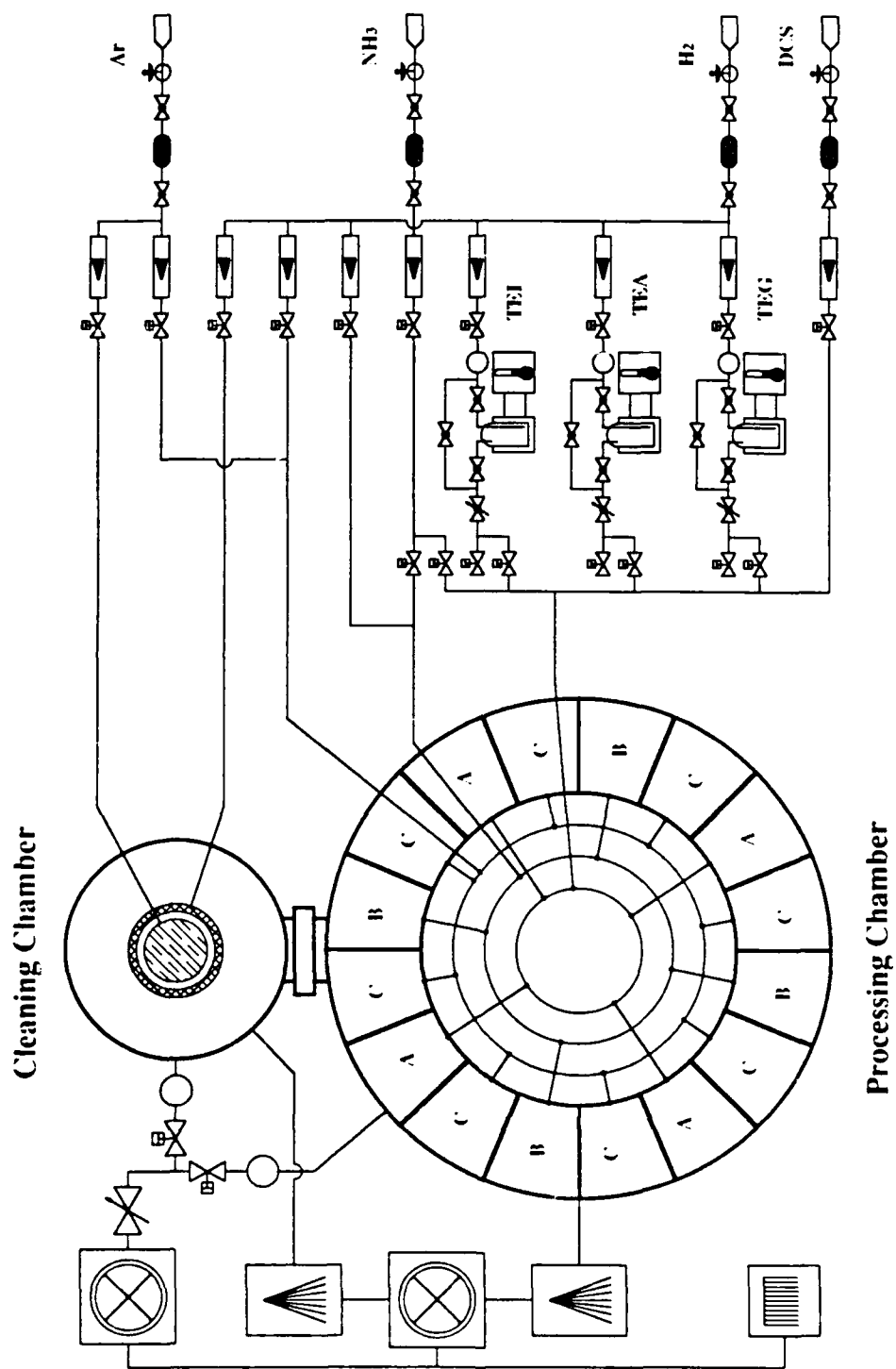


Figure 3. A block diagram of the nitride ALE system. Legend given on next page.

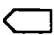










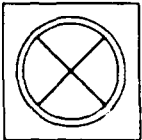
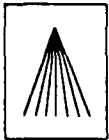

	Gas cylinder
	Regulator and cross-purge assembly
	Chemical gas purifier
	Manual shut-off valve
	Mass flow controller
	Pneumatic shut-off valve
	Capacitance pressure gauge
	Manual metering valve
	Organometallic bubbler
	Constant temperature bath
	Automatic butterfly valve
	Rotary vane pump
	Diffusion pump
	Scrubber

Figure 3a. Legend for Figure 3.

temperature,  $P_{OM}(T)$ , and the partial pressure of the carrier gas (= total pressure ( $p_t$ )- $P_{OM}(T)$ ).

$$X_{OM}(T) = \frac{P_{OM}(T)}{p_t - P_{OM}(T)}$$

The exact number of moles of OM introduced into chamber may then calculated from the known flow rate of the carrier gas.

The control of the introduction of the gaseous sources is much simpler: a mass flow controller with a shut-off valve.

The pumping system consists of two diffusion pumps, one each for the cleaning and process chambers, and two rotary vane pumps. One of the latter serves as a backing pump for the diffusion pumps and the other as the process pump. Both diffusion pumps are used to achieve the ultimate pressure and to insure a clean process environment (i.e. a low pressure of background contaminants) but are not used during the deposition. The volatile exhaust gases are diluted with nitrogen and cleaned in a water scrubber prior to their release into a central exhaust system.

*Growth Theory.* Several different precursors have been considered for the ALE of GaN. After much study, organometallics were selected for the column III source-materials and ammonia as the nitrogen source. Organometallic sources have been chosen over chlorides because of their high purity, ease of transport from the source to the chamber and excellent control over dosing. Triethyls were chosen over trimethyls for two reasons: (1) lower decomposition temperature and thus lower growth temperature, which can potentially reduce the concentration of nitrogen vacancies, and (2) cleaner surface reaction (trimethyls have been known to leave high carbon residue at the higher deposition temperatures, which become incorporated in the growing film). Ammonia has been chosen over hydrazine and nitrogen fluoride mainly because of safety considerations and cleanliness. Ammonia is available in research grade purity. Ammonia purifiers, which effectively remove the remaining water, oxygen and carbonyl compounds, are also available.

The reaction energy budget these precursors offer theoretically favors the self-limiting ALE deposition of III-V nitrides on (0001) surfaces of the wurtzite or (111) surfaces of zincblende substrates. The growth direction is crucial, because the number of bonds a particular species makes on the surface varies greatly with the growth direction. A constituent of a tetrahedrally bonded compound can make one surface bond in the  $000\bar{1}$  direction, two surface bonds in (1011) direction and three surface bonds in the 0001 direction. The last two cases are shown in Figures 4(a) & (b).

An estimate of whether a reaction is favored or not can be made by comparing the bond energies of the reactants and the products. The bond energies between Group III metals and nitrogen, calculated using different methods, are summarized in Table I.

## (100), (1011) and (111), (0001) Surface Bonds in ZB, W Crystals

- grow on high density planes (111, 0001) having polarity which more strongly bonds nitrogen (3 bonds with metal)
- this also makes surface metal species more mobile (surface metal makes only one bond)

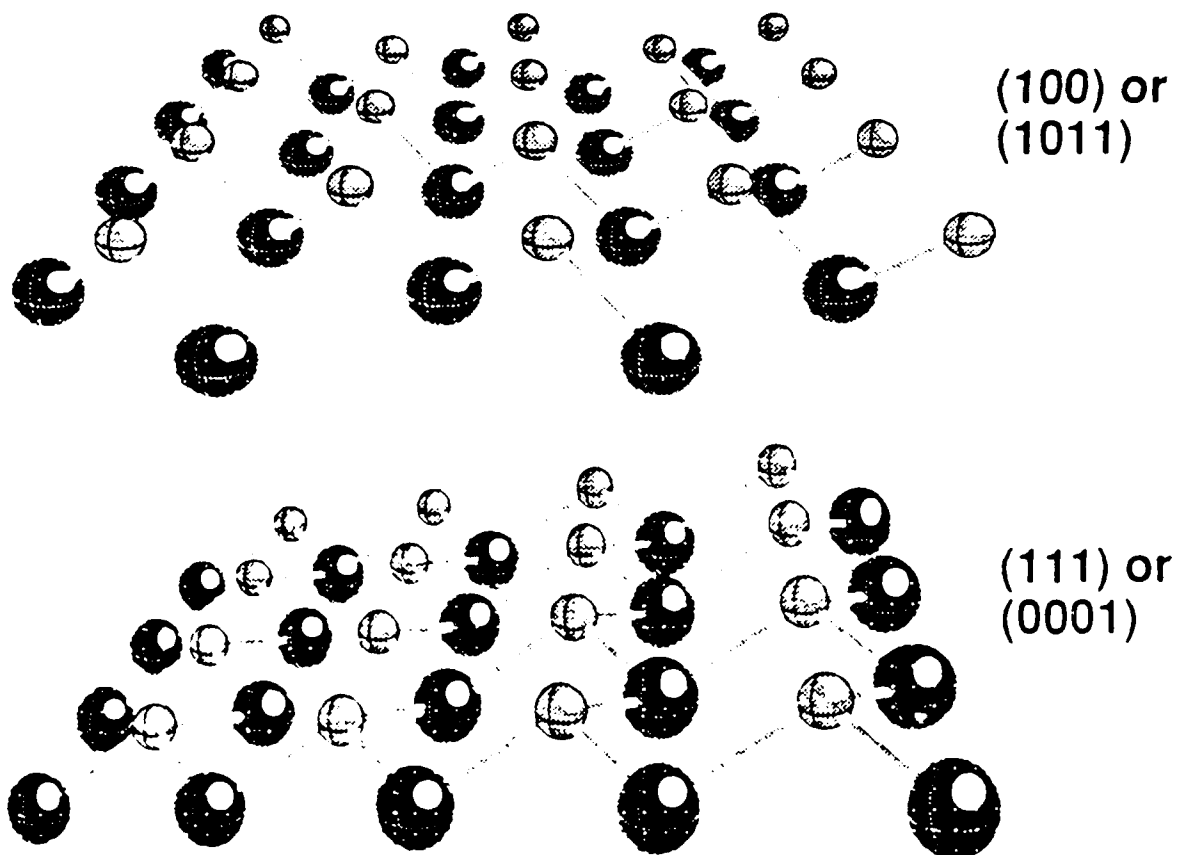


Figure 4. Surface bonds in two different growth directions in cubic and hexagonal tetrahedrally bonded crystals: a) (100) or (1011), and b) (111) or (0001).

Table I. Bond energies between Group III metals and nitrogen obtained by different methods.

B - N	Al - N	Ga - N	In - N	Remarks
93±5	71±23	87	*	Tabulated values [5]
115	125	108	105	Pauling's formula [6]
94	90	65	54	Geometrical mean with correction [6]
83-193	52-122	55-85	47-67	Immediate neighbors
72-91	64-80	55-69	49-61	Periodic behavior
66	67(81)	50(56)	49	Heat of vaporization [7]
87	94	69	58	Heat of formation [8]
<b>85±5</b>	<b>75±5</b>	<b>65±5</b>	<b>55±5</b>	Suggested values

Suppose, the (0001) surface is saturated with the  $\text{Ga}(\text{C}_2\text{H}_5)_2$  species, which make one bond with the underlying nitrogen. When such a surface is exposed to ammonia, a reaction will occur if making three bonds with Ga is energetically favorable for the nitrogen of the ammonia molecule. The process will end with a hydrogen terminated surface, which does not react further with ammonia. The bond energy between Ga and the ethyl radical is 57 kcal/mol, and the average bond energy between nitrogen and hydrogen is about 90 kcal/mol. To make three new bonds on the surface, one needs  $3 \times 57 + 2 \times 90 = 351$  kcal/mol. On the other hand, production of one N-Ga bond releases 65 kcal/mol, and the reaction  $\text{C}_2\text{H}_5 + \text{H} \rightarrow \text{C}_2\text{H}_6$  produces about 100 kcal/mol. Thus the total energy produced equals to:  $3 \times 65 + 2 \times 10 = 395$  kcal/mol. Since the energy produced is larger than the energy consumed, the reaction is favorable.

A similar calculation can be done for the next, Ga layer. The Ga cycle starts with a hydrogen terminated nitrogen surface. Arriving TEG chemically adsorbs on the surface by breaking one H-N bond (90 kcal/mol) and one Ga-Ethyl bond (57 kcal/mol) and making one Ga-N bond (65 kcal/mol) and one C-H bond (100 kcal/mol) producing  $\text{C}_2\text{H}_6$ . The energy balance is 147:165 and reaction is again favorable.

The same calculation is valid also for AlN and BN. The only III metal with a marginal outcome is In, as can be seen from the data in Table I. However, such calculations offer only a rough estimate, since data on bond energies are not very accurate. Moreover, the change of state from gas to solid has been neglected. Energy requirements on a surface which acts as a catalyst may be even lower.

*Growth and Analysis Procedures.* In order to test and characterize the new equipment and processes, several deposition runs were made using different growth parameters. Table II gives the ranges in which the various parameters were varied. Throughout the test depositions four out of sixteen zones were used for TEG, four for ammonia and eight for the hydrogen purge gas.

---

Table II. Growth parameters.

---

Growth temperature	350 - 650°C
Growth pressure	0.5 - 50 Torr
Ammonia flow rate	100 - 300 sccm
H <sub>2</sub> (purge) flow rate	200 - 300 sccm
H <sub>2</sub> (OM carrier) flow rate	50 - 100 sccm
TEGa bubbler temperature	-10 - 20°C
TEGa bubbler pressure	400 - 800 Torr
Rotation speed	1 - 2 RPM

---

Reflectron High Energy Electron Diffraction (RHEED) was performed on the grown films to determine the crystallinity and structure. Scanning Auger microscopy (JEOL JAMP-30) was performed to determine the presence of impurities and nominal composition of the GaN layers. Scanning electron microscopy (Hitachi S-530) was performed to evaluate the surface morphology of the deposited thin films.

### C. Experimental Results and Discussion

*Surface Morphology.* Initially, a few CVD runs were attempted, where all reactants were introduced into the same growth zone. The substrate temperatures were rather high, 750–850°C, and the process routes did not result in the growth of any GaN films. Only large (>10 μm) individual GaN crystals were observed on the surface, as shown in Figures 5(a) & (b). They are a possible result of homogeneous nucleation in the gas phase.

After a few unsuccessful experiments, the reactants were separated and distributed to different growth zones. The substrates were rotated and sequentially exposed to different reactants. Films were grown at constant chamber pressure of 50 torr, while other parameters such as, growth temperature, flow rates, and the rotation speed were changed.



Figure 5. An AFM image of GaN crystals obtained with CVD growth shown at two different magnifications. The growth temperature was 810 °C.

Figures 6, 7 and 8 show the surface morphology of three GaN films grown under different conditions. Figures 6(a) & (b) shows a film grown at 560°C. Note the much higher nucleation density than in Figure 5. Figure 6(b) has been taken close to an edge of the wafer, where the nucleation density was low, and the individual crystallites were clearly seen. All of them have either a hexagonal or a triangular shape, both of which indicate a hexagonal structure. All of them are also oriented in the same direction; note, that all {0001} planes are perpendicular to the surface and {1010} planes of the individual crystallites are parallel among each other. This indicates a good epitaxial relationship with the  $\alpha(6H)$ -SiC (0001) substrate.

Figure 7 shows the surface of a GaN film grown at 390°C. The film is continuous, as confirmed by chemical analysis. The ovals on the surface of the film are conglomerates of unreacted gallium. Apparently TEG decomposes at this temperature effectively; however, the concentration of ammonia is insufficient for complete reaction. When the supply of TEG was reduced by about three times, a clean GaN film without Ga precipitates was obtained, as shown in Figure 8. However, this procedure also reduced the growth rate from 2000 Å/hr to 600 Å/hr.

*Chemical Analysis.* Scanning Auger microscopy was performed on the samples to determine the presence of impurities and the nominal composition of the GaN layers. Figure 9 shows an Auger spectrum taken from the untreated growth surface. The oxygen and carbon peaks are due to surface oxidation and contamination upon exposure to the atmosphere. No other contaminants were observed to the resolution of the instrument (typically  $\approx 0.1$  at.%).

An Auger depth profile was also obtained and is shown in Figure 10. The profile shows that indeed the oxygen and carbon contamination was only on the surface. The apparent low nitrogen content of the film is in part due to the relative elemental sensitivity factors. Another factor may possibly be a result of the sputtering action of the 3 kV Ar<sup>+</sup> ions. A similar effect has been seen in InN<sup>9</sup>.

*Electron Diffraction.* Reflection high-energy electron diffraction (RHEED) was performed on GaN films. Films grown at 350°C and lower showed only a diffused ring diffraction pattern and were apparently amorphous. Films grown at 380°C or higher showed a distinct diffraction pattern indicative of the wurtzite structure. Diffraction patterns of a film grown at 390°C and taken in two different directions are shown in Figure 11. Although Kikuchi lines were observed which are the fingerprint of good crystallinity, the surface of the film appears to be rough, as shown by the spotty diffraction pattern.



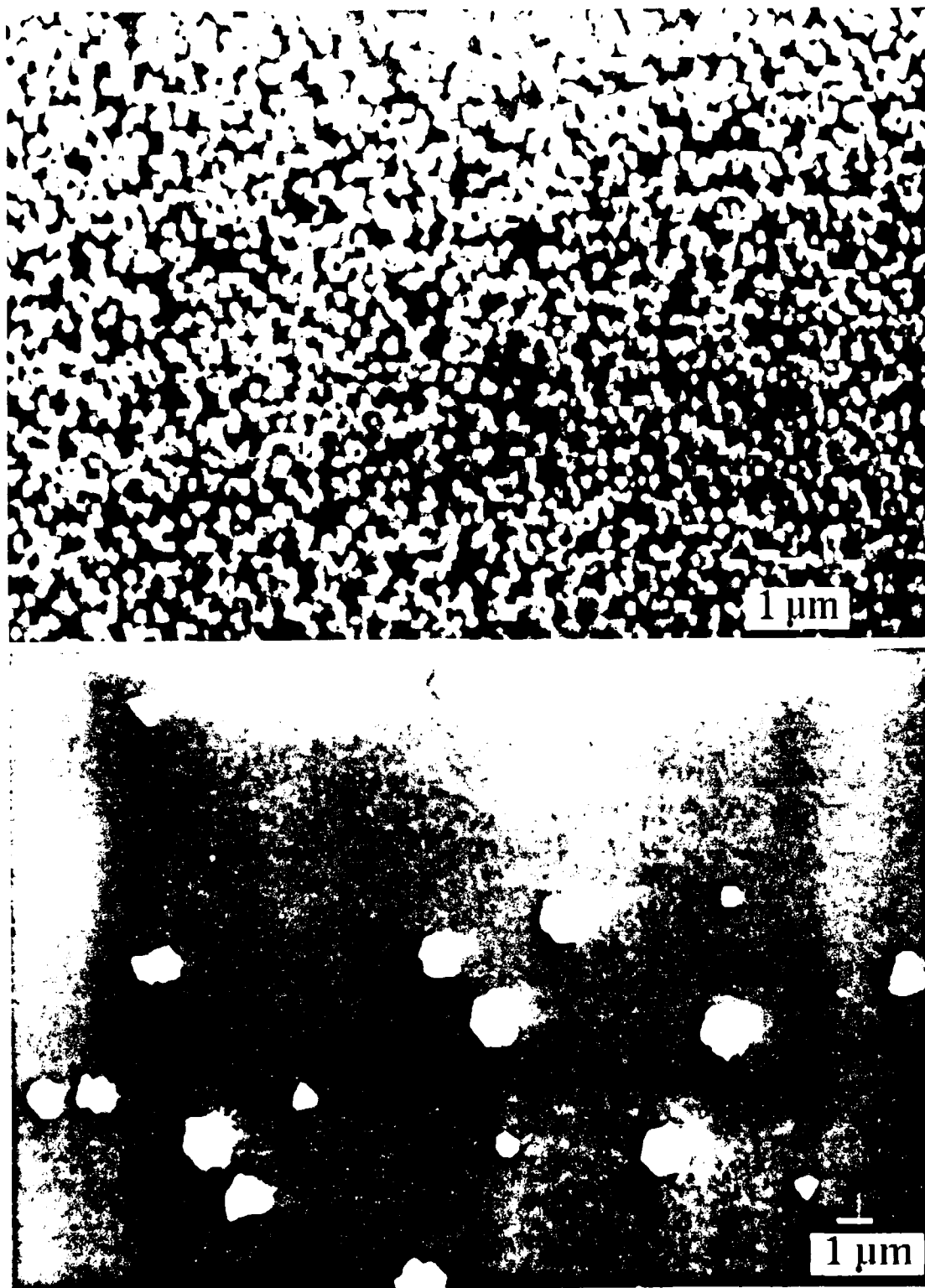


Figure 6. a) Surface morphology of GaN on a-SiC grown at 560 °C. Note a much higher nucleation density than in Figure 5. b) A micrograph taken at the edge of the same wafer, where the nucleation density was low. Note the perfect orientational relationship between individual crystallites.

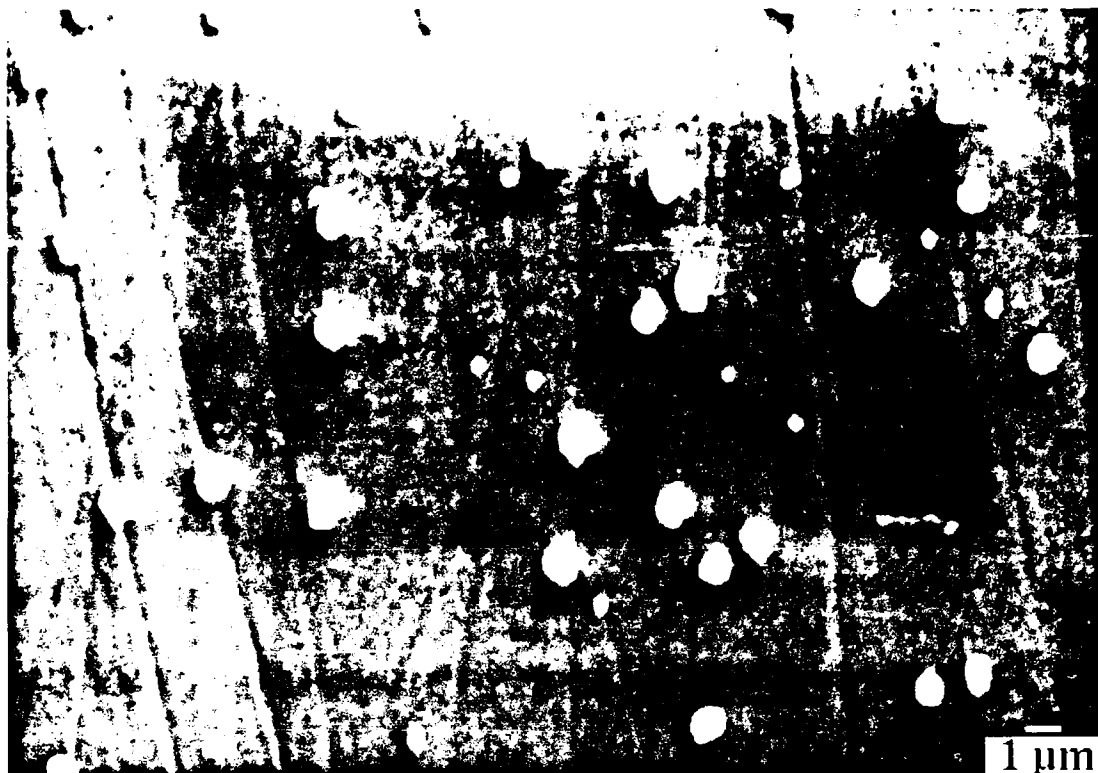


Figure 7. A micrograph of GaN film grown at 390°C on  $\alpha$ -SiC. Film is continuous, but there is excess Ga on the surface.

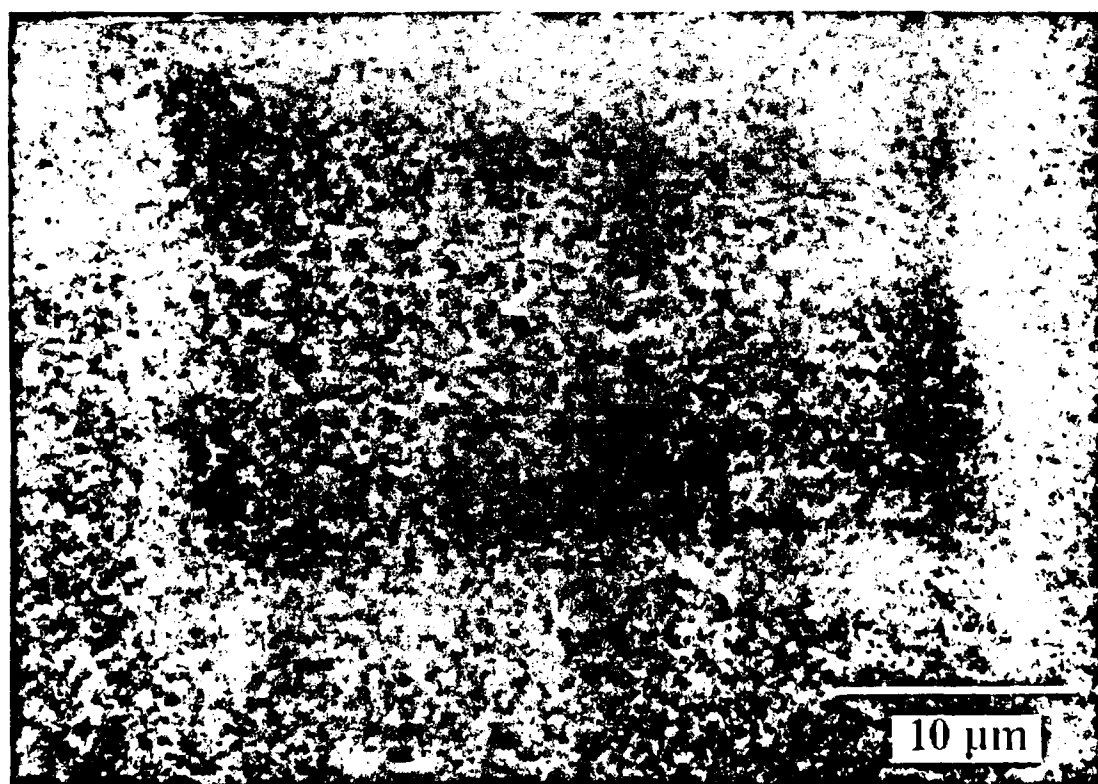


Figure 8. The surface of an as grown ALE GaN film, after TEG flow rate was reduced. No excess gallium was observed on the surface and RHEED showed good crystallinity.

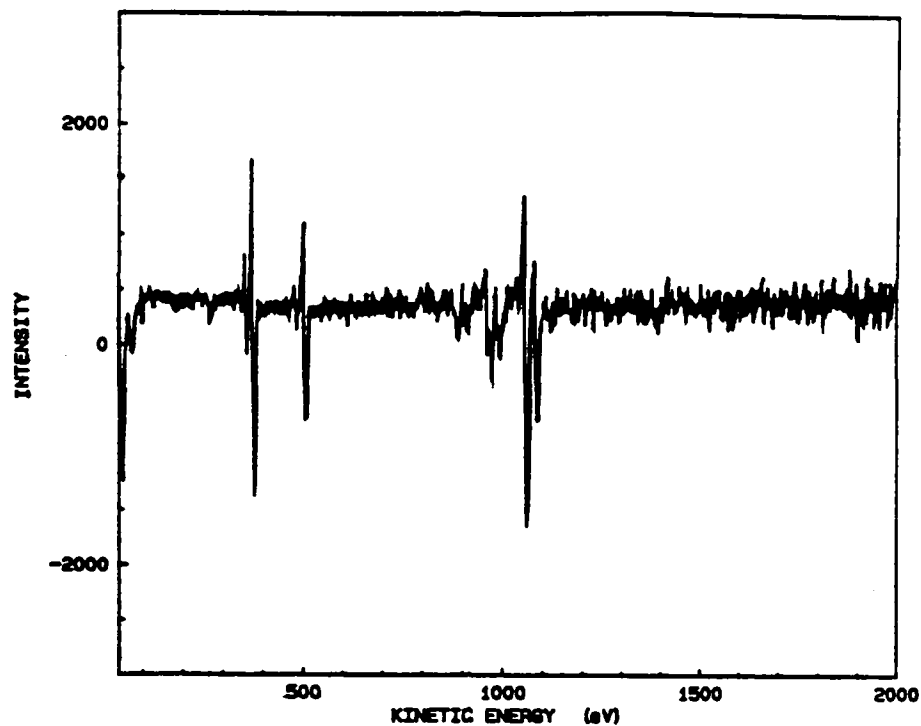


Figure 9. Auger spectrum taken from the untreated GaN surface. Only oxygen and carbon contamination was detected, which is due to exposure to the atmosphere.

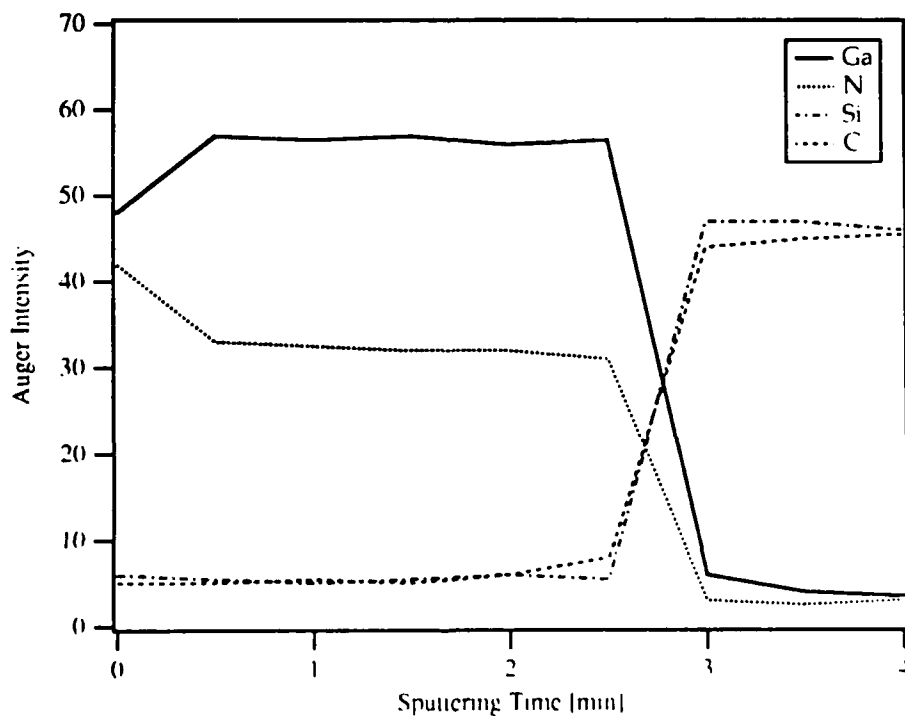


Figure 10. Auger depth profile of GaN on  $\alpha$ -SiC (0001). Oxygen and carbon contamination was detected only at the surface.

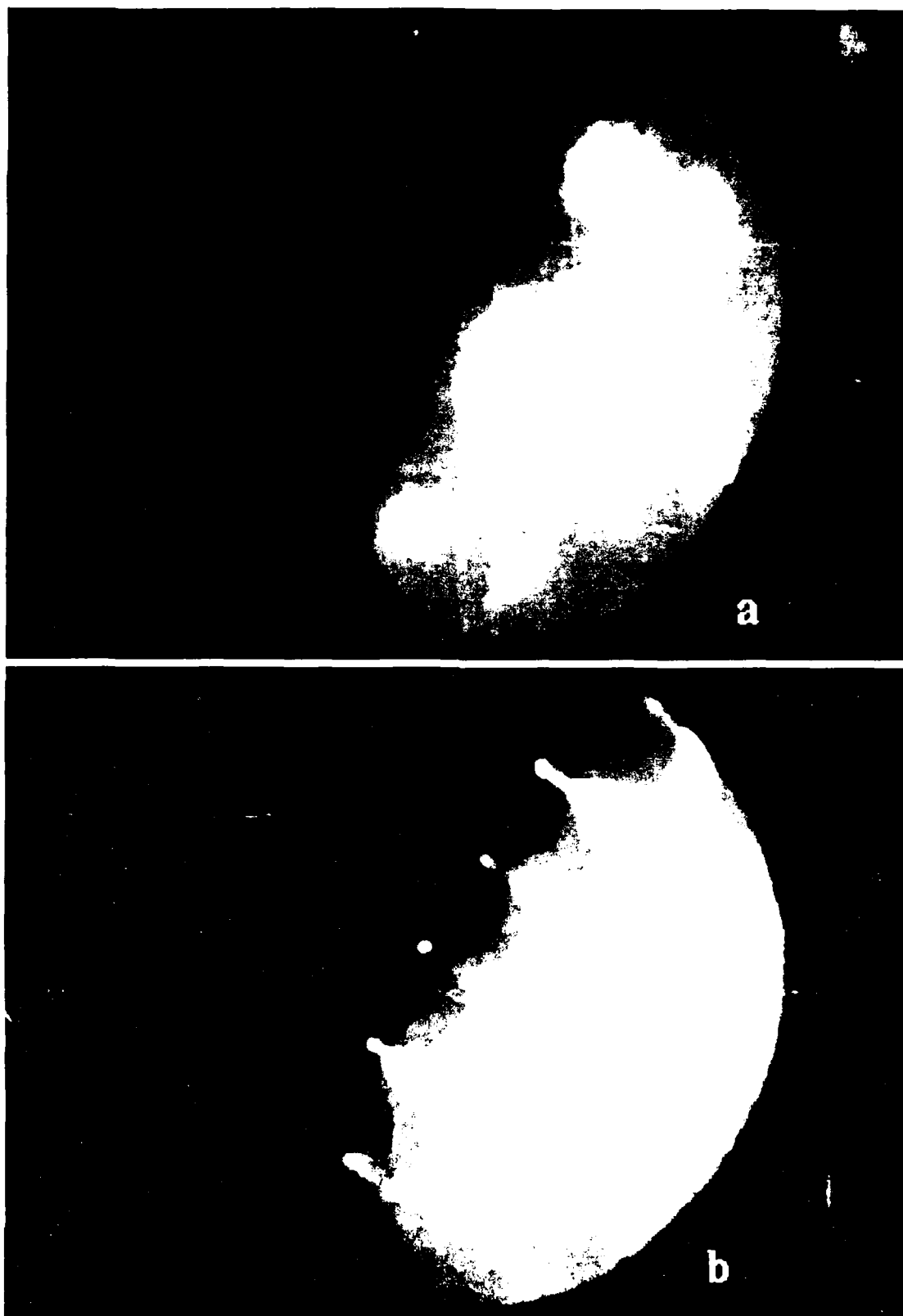


Figure 11. RHEED pattern of a GaN film grown on (0001)-a SiC by ALF: (a)  $[01\bar{1}0]$ , (b)  $[2\bar{1}\bar{1}0]$ .

#### D. Conclusions

The initial results of the ALE growth of GaN are very encouraging. The system has been performing in a satisfactory manner. Although the growth results are improving from run to run, the self-limiting ALE growth regime has not yet been achieved.

Apparently ammonia does not react very efficiently at the present growth temperatures. To promote the reaction, tungsten cracker filaments were installed in each ammonia zone. These filaments will run at 800–1200°C which is much higher than the substrate temperature and should greatly enhance the reactivity of ammonia.

#### E. Future Research

The research on the ALE of GaN will be continued. A similar process for AlN and their solid solutions and heterostructures will also be determined and employed. The conditions for a self limiting process in the growth of all III-V nitrides will be investigated. The effectiveness of the ammonia decomposition in the cracker filaments on the low temperature ( $\leq 350^\circ\text{C}$ ) deposition of stoichiometric GaN and AlN will also be determined.

## II. GROWTH OF CUBIC BORON NITRIDE

#### A. Introduction

Boron nitride has long been known for its desirable properties as a highly insulating as well as a chemically and thermally stable material. Thin films of cubic boron nitride (C-BN) have many potential applications in areas such as diamond substrates and optoelectronic devices in the vacuum ultraviolet. The cubic phase was first reported by Wentorf,[10] who produced it in a high pressure apparatus and even made the initial measurements on the material's semiconducting properties. It has been used since then primarily for its high hardness in applications such as grinding and polishing. The cubic phase of BN is actually the zinc blende structure or in space group notation  $F\bar{4}3m$  (Hermann-Mauguin) or  $T_d^2$  (Schöenflies). Boron nitride is very similar to carbon in that both exist in hexagonal, wurtzitic, and cubic forms and many of the properties in each of the phases are strikingly similar. The rare exception is that hexagonal boron nitride is an insulator and hexagonal carbon is a conductor. Among the many similarities include the fact that both diamond and c-BN are metastable under the conditions currently used for growth of thin films.

Interest in the cubic polymorph of BN as a semiconductor material has received much interest recently as a possible substrate for the deposition of diamond, due to the similar lattice parameters ( $\Delta a_0 = 1.34\%$ ) and its wider bandgap which is in the range of 5.8–6.5 eV.[11–13] The very wide bandgap of c-BN also gives c-BN applications in its own right, as optical devices for the vacuum UV ( $\lambda \sim 200$  nm). For a complete listing of materials-related properties

of c-BN see *Landolt-Börnstein: Numerical Data and Functional Relationships in Science and Technology, Series III, Vols. 17 and 23*, or Ref. [14] (which also includes a side-by-side comparison of properties of c-BN with diamond).

Several approaches have been employed in the attempt to grow thin films of cubic boron nitride (c-BN). These include reactive diode[15] and rf sputtering,[16] ion implantation,[17, 18] plasma CVD,[19–21] microwave plasma CVD,[22, 23] and ion plating techniques.[24–27] These attempts were successful in producing polycrystalline films of c-BN, predominantly of a mixed nature with both cubic and other phases present and of extremely fine grain size. It appears that most researchers succeeded in the deposition of c-BN if the technique included the input of additional energy from energetic ions during the deposition process.

## B. Selection of Substrate Materials, Deposition Technologies and Analytical Techniques

*Substrate Materials.* In the present study, film growth has been attempted primarily on single crystals of silicon and copper. Silicon was chosen since it is well characterized and understood, readily available in single crystal form, and nearly all previous studies have included silicon as a substrate. Additionally, it is a technologically important material for heteroepitaxy of c-BN in microelectronic applications. There is also some evidence that indicates that despite the high lattice mismatch of c-BN→Si ( $\approx 33\%$ ), a much lower strain ( $\approx 4\%$ ) atomic coincidence boundary does occur,[28] which might permit high quality layers to be produced with Si as a substrate.

Copper was chosen primarily because of its near perfect lattice match ( $\Delta a_0 = 0.022\%$ ). The thermal expansion difference is slight ( $\approx 10$  ppm/ $^{\circ}\text{C}$ ) and actually improves the lattice match at growth temperatures. Copper does form a nitride ( $\text{Cu}_3\text{N}$ ) which could pose a problem at the growth interface, but it decomposes above  $300\text{--}400^{\circ}\text{C}$ ,[29] and its lattice parameter ( $3.815 \text{ \AA}$ )[30] is only  $\approx 5\%$  larger than c-BN. Since growths have taken place at higher temperatures ( $500\text{--}700^{\circ}\text{C}$ ), formation of an interfacial phase which might interfere with the growing layer is not expected. Surface energy difference is a problem, as copper has a much lower surface energy than c-BN ( $1430$  vs.  $4770 \text{ erg/cm}^2$ ).[14, 31] This problem plagues c-BN heteroepitaxial deposition in every case except c-BN on diamond. This problem will be discussed further in the section on Future Research.

*Deposition Technologies.* Gas source molecular beam epitaxy (GSMBE) was chosen for several reasons. The UHV conditions of the system provided very clean background conditions for growth. Many if not all of the films grown in previous studies contained oxygen in the films and contamination is a serious problem for electronic materials. The *in situ* capability of RHEED as well as the additional in vacuum analytical techniques of LEED

and XPS, permit careful evaluation of the film before degradation upon exposure to the atmosphere.

The compact ECR source (described briefly in the Experimental Procedure and in detail in Ref. [32]) produces excited as well as ground state species within the intense plasma conditions of the source. The presence of these excited species is important to the formation of the metastable cubic phase. Since the difference in enthalpy of formation between the hexagonal and cubic phases is small ( $\approx 3.63$  kcal/mol @ 25°C), the primary problem is a very high activation barrier between the phases. Use of these excited state species is important to overcoming this barrier. However, very high kinetic energy species are not desired as they will produce many defects in the growing layer. This problem will be discussed further in the section on Future Research.

Microwave plasma CVD was also investigated as a potential method of depositing c-BN films since some investigators had used it successfully in producing partially c-BN films and might be successfully extended to single crystal films. An agreement was reached with ASTeX, Inc., in Boston, MA, whereby one of their microwave plasma CVD systems was adapted for BN deposition. This involved installing a new mass flow controller and a bottle of borazine liquid into the gas handling system. For the depositions, M. J. Paisley went to ASTeX, Inc., and worked with Mr. Larry Bourget of ASTeX in setting process parameters and performing the depositions.

*Analytical Techniques.* XPS, RHEED, and LEED are *in vacuo* techniques for the MBE system and thus are natural choices for films grown in that system. RHEED (for review of the use of RHEED see Ref. [33]) and LEED (described in detail in Ref. [34]) are very sensitive techniques for determining crystal structures and can also give information regarding certain details of surface morphology. XPS gives information regarding chemical purity and some information regarding chemical state of constituent species. This is not particularly true for nitrogen, as its electronegativity (only oxygen, chlorine and fluorine are higher) results in only very minor shifts in peak position as a function of stoichiometry.[35] XPS can potentially also give structural information through the plasmon loss features associated with the elemental peaks.[36]

X-ray diffraction and TEM also give very good structural information, x-ray diffraction on a much broader scale than RHEED and LEED, while TEM is on a much finer scale of structure. In addition, TEM and SEM give detailed structural and morphological information on the films and substrates.

Additional purity and local structure information can be obtained from transmission FT-IR measurements. The infrared region corresponds to excitation of phonon modes in the material for bond stretching and bond bending processes.[37] These energies are unique for each type of bond, so that B-N bond stretching can be differentiated from B-H bond

stretching, etc. This differentiation allows FT-IR to determine presence of contaminants in general, and an ability to detect hydrogen, which is difficult by most analytical methods. Since some of these bond excitation processes are three-dimensional in nature and are restricted in their degrees of freedom by the surrounding crystal lattice, FT-IR also provides local structural information which can indicate the structure of the surrounding lattice.[38]

Silicon is an excellent substrate material for FT-IR measurements since it is transparent in the infrared region scanned ( $400\text{--}4800\text{ cm}^{-1}$ ,  $0.05\text{--}0.6\text{ eV}$ ,  $\lambda=25\text{--}2\text{ }\mu\text{m}$ ). For these reasons, transmission FT-IR has been used by many researchers[21, 22, 27, 39–42] as a non-destructive technique for observing the cubic and hexagonal or amorphous phases of deposited BN films.

Raman spectroscopy excites the same phonon modes in the material as infrared spectroscopy though via different processes. Whether a phonon mode is infrared or Raman active (or both or neither) is dependent upon whether or not creating (or destroying) that phonon would change the dipole moment or electronic polarizability, respectively, of the crystal. Since the lattice site symmetry of the molecule is different in different crystal structures, Raman and/or infrared spectroscopy can be used to determine crystal structures.[37, 38] This can be critical in cases of single crystal films as certain phonon modes can be suppressed when analyzing samples in specific orientations.[43]

### C. Experimental Procedures

*Gas Source MBE.* The primary deposition technique was GSMBE wherein elemental boron is evaporated from a high temperature effusion cell and molecular nitrogen gas is passed through a compact electron cyclotron resonance (ECR) plasma source to activate and dissociate the nitrogen. The growth system was a Perkin-Elmer 430 MBE system modified as described below. It consisted of three major sections: a load lock (base pressure  $\approx 5 \times 10^{-8}$  Torr), a transfer tube (base pressure  $\approx 3 \times 10^{-10}$  Torr) which was used to degas the substrates, and the growth chamber (base pressure  $\approx 1 \times 10^{-10}$  Torr). The growth chamber was equipped with four standard 20 cc effusion cells that contained BN crucibles which were resistively heated with Ta wire heaters used in research of other nitrides.

One modification was the addition of a special high temperature effusion cell. This cell uses a W3%Re-W26%Re thermocouple and a tungsten alloy heater filament which is driven by a 2700 W DC power supply. It mounts on a standard 4.5" metal seal flange along with all the other metal evaporation sources. A BN crucible was used as it was believed that slight decomposition of the crucible at the elevated operating temperatures would not affect the growth of BN films. Prior to installation of the source, the BN crucible was loaded with 3 g of 99.9999% pure boron.



The more significant modification was the use of a compact ECR microwave glow-discharge plasma to dissociate/activate the N containing gas. This source was designed and commissioned in an in-house effort by Dr. Zlatko Sitar.[32] This source has the advantages of fitting inside the nominal two-inch diameter tube of the source flange cryoshroud and thus minimize the source to substrate distance. As a result, the flux of activated/dissociated species arriving at the substrate surface is increased. This source was attached in place of a more traditional effusion (or cracker) cell for the group V element. The nitrogen gas was taken from a bottle of compressed UHP-grade nitrogen, purified by a metallorganic resin bed gettering material and subsequently regulated to the source by a variable leak valve.

Some depositions also included use of borazine ( $B_3N_3H_6$ ) in a nitrogen carrier gas as both a source for boron and for nitrogen. Borazine was chosen as a gas source for boron to investigate activation of the source of boron in the ECR plasma as well as an attempt to determine if boron-nitrogen compounds provide a more suitable precursor since the B-N bond already exists in the material. This was done by placing the borazine (which is liquid at STP) in a temperature controlled bubbler and passing nitrogen gas through it which then passed into the ECR source.

Substrate preparation involved a 30 min. exposure to UV which has been shown to remove hydrocarbon contamination,[44] followed by a dilute acid etch to remove oxide layers. In the case of Si, a solution of  $H_2O:HF$  (10:1) was used,[45] and for Cu, a solution of  $H_2O:HCl$  (10:1) was used.[46] Subsequently, the substrates were mounted on a Mo holder using either molten indium or silver paste. Silver paste was very important for the copper substrates as they were extremely sensitive to oxidation and would oxidize heavily in attempting to indium bond the substrates.

Samples were then loaded into a cryopumped load lock. After the initial evacuation, the samples were loaded into the transfer tube where they were degassed to a temperature of 700°C. Immediately after degassing they were loaded into the growth chamber and the deposition cycle began. Typical deposition conditions used are shown in Table I.

---

Table I. Deposition Conditions used in GSMBE of BN

---

Nitrogen pressure	$1-2 \times 10^{-4}$ Torr
Microwave power	20-50 W
Boron temperature	1725 - 1775°C
Borazine temperature (where used)	-10°C
Substrate temperature	600 - 700°C
Growth time (BN)	120 - 360 min.
Deposited film thickness	10-850 Å

---

Subsequent to deposition the sample would either be moved to the load lock for removal from the system or transferred to the analytical system for additional characterization.

*Microwave Plasma CVD.* The microwave plasma CVD system consisted of a gas manifold where gases could be injected directly into the plasma or downstream from it. Depositions were performed in two modes: (1) borazine, nitrogen and argon were introduced in the plasma, and (2) argon and nitrogen were injected into the plasma and the borazine was injected downstream. The substrate support was isolated making it possible to add rf biasing to the substrate to increase ion bombardment from the plasma. A schematic diagram of the ASTeX system is shown in Figure 12.

Substrates of Si (100) or Si (111) along with quartz and tool steel were placed into a load lock and evacuated before loading into the main deposition chamber. Then the samples were heated under vacuum until the deposition temperature was reached. Finally, gas flow was begun and the plasma was ignited and deposition commenced. In situations where substrate bias was used, the plasma was initiated and stabilized then the bias conditions established and finally deposition began. After deposition, the samples were cooled and removed for ellipsometry and eventual further analysis at NCSU. The range of conditions used for deposition is shown in Table II.

Table II. Deposition Conditions used in MWCVD of BN

Borazine flow	1.5 – 10 sccm
Nitrogen flow	0 – 20 sccm
Argon flow	0 – 50 sccm
Chamber pressure	0.9 – 5.0 mTorr
Microwave power	500 – 1000 W
Substrate temperature	590 – 620°C
Substrate rf-induced voltage	0 to –65 V
Growth time (BN)	3 – 30 min.
Deposited film thickness	50 – 2000 nm

Some readers might be confused by the entry for *Substrate rf bias voltage* listed in Table II. When the rf bias was applied to the substrate, the presence of the plasma caused a DC bias to be induced on the substrate surface. This bias resulted in ions being accelerated to the substrate surface. This induced bias is a much more descriptive measure of the effects of the rf biasing than the measure of rf bias power applied, and thus is used instead of the power. (Note: This rf bias was measured simply by attaching a voltmeter between ground and the substrate holder with the addition of a low-pass filter to protect the voltmeter from rf voltages.)

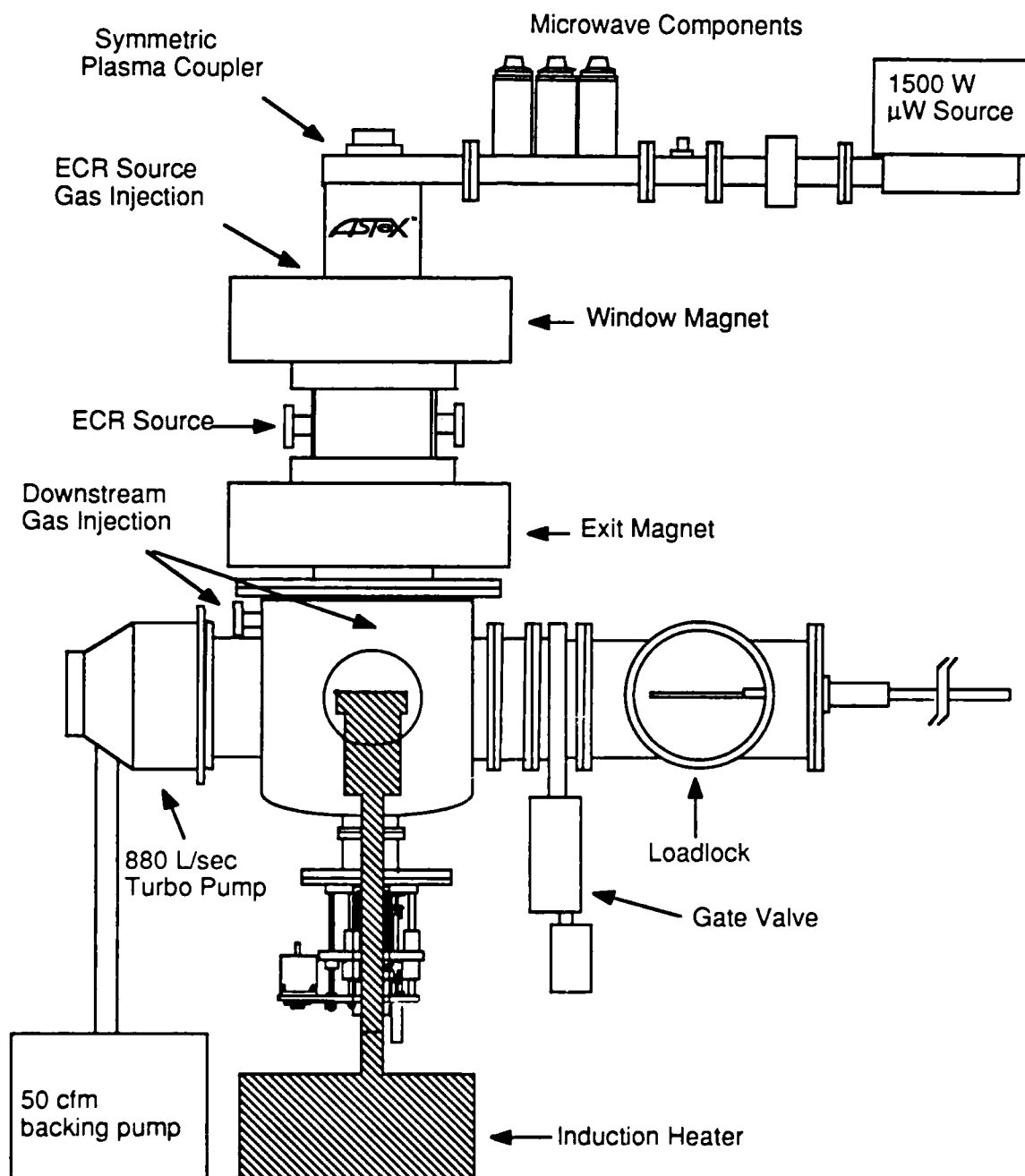


Figure 12. Schematic diagram of microwave plasma CVD system used at ASTeX, Inc. to deposit BN films.

## D. Results

### Gas Source MBE

BN on Silicon (100) Substrates. The BN films grown on silicon substrates exhibited very good chemical purity but poor crystal structure definition as was shown in the previous progress report of December, 1990. Only new and additional results will be reported here.

Infrared spectroscopy (FT-IR) can be used to give further chemical and structural information on the deposited layer. Arrangements were made to perform FT-IR measurements in the Textile Engineering, Chemistry, and Science Department here at NCSU. Shown in Figure 13 is an FT-IR spectra showing absorption features of the BN film after background subtraction for the Si substrate and atmospheric absorption effects.

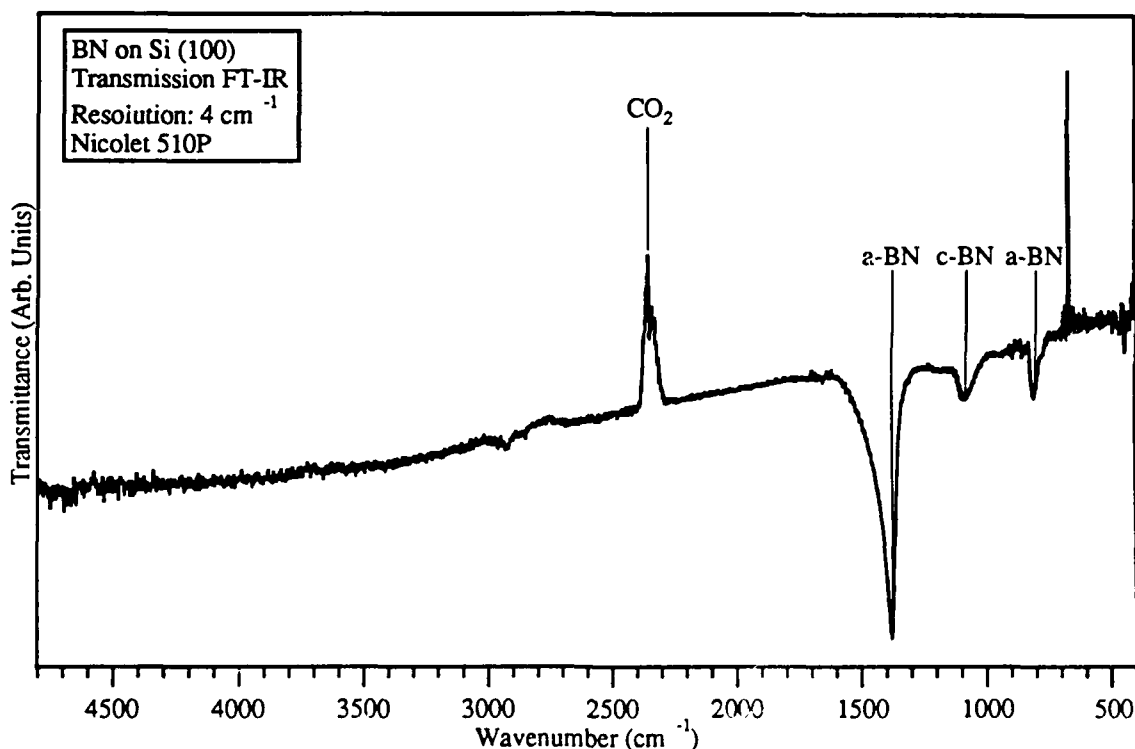


Figure 13. Transmission FT-IR spectra of BN deposited on Si (100) substrate. Inverted CO<sub>2</sub> absorption peak is present because concentration was lower when analyzing sample than for instrument baseline spectrum.

Copper Substrates. Analyses of the initial copper substrates (99.999% pure) were undertaken to determine the initial purity of the substrate surface as well as its surface structure. Figure 14 shows the Auger electron spectrum of the substrate surface after 700°C vacuum anneal. Note that no oxygen and only a trace of carbon are observed, indicative of good substrate preparation prior to evacuation. The sulfur peak and some of the copper peaks appear as doublets indicating that the sulfur is present in two different states. There is no

chlorine present which is observed in HCl-etched copper,[46] probably due to removal of the chlorine from the surface in the vacuum annealing stage.

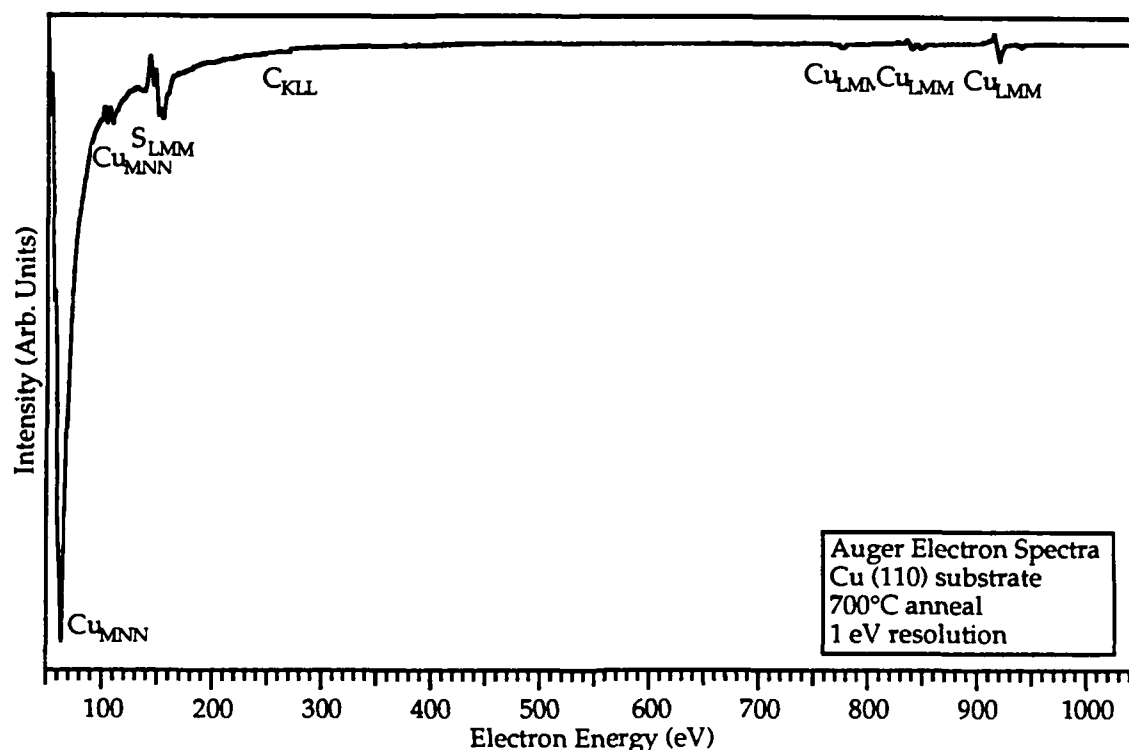
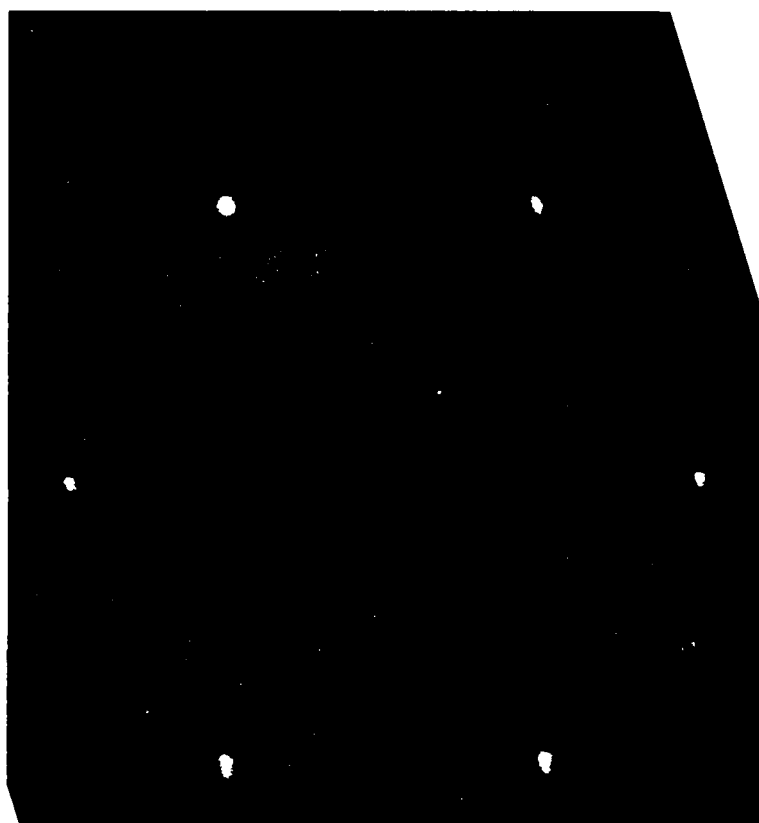


Figure 14. Auger electron spectrum of Cu(110) substrate. Note presence of sulfur (doublet) and trace of carbon contamination.

To determine the degree of surface order, LEED patterns were taken at several different voltages. Shown in Figures 15 and 16 are two of the LEED patterns observed from the Cu(110) surface. Note that several fractional order beams are observed clearly in Figure 15 and this pattern is tentatively assigned (1×1) with additional spot splitting.

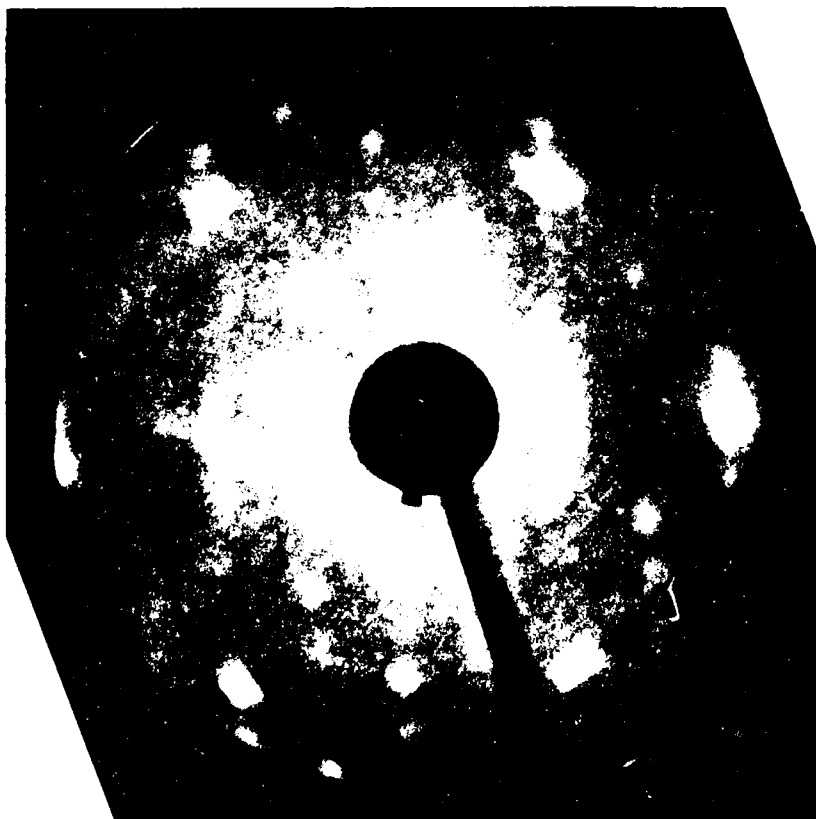
This is more clearly observed in Figure 16, where a more complete but more diffuse pattern is observed. The more complete pattern is due just to the decrease in electron wavelength as the electron energy is increased.

High resolution field emission SEM (Hitachi S-4000) photographs were taken to determine the quality of the initial growth surface of the Cu substrates. Figure 17 shows both low and high magnification images from the substrate surface. The relatively smooth surface is apparent, except for occasional scratches and a very fine texturing observable only at high magnification. Some small dimples were also observed in the surface from the electrochemical polishing step (not shown) which were widely separated.



$[001]$   $\bullet$  — — — — —  $\bullet$   
 $[110]$

Figure 15. LEED pattern observed on Cu (110) substrate before deposition and after a 700 °C / 7 hK anneal showing the basic (110) pattern with a few reconstruction spots (Beam: 26.5 Å)



$[001]$   $\bullet$   
 $[110]$

Figure 16. LEED pattern observed on Cu (110) substrate after deposition of a 2 nm thick layer of Pt and annealing at 700 °C / 7 hK. The pattern shows a more complex structure with many reconstruction spots (Beam: 26.5 Å)

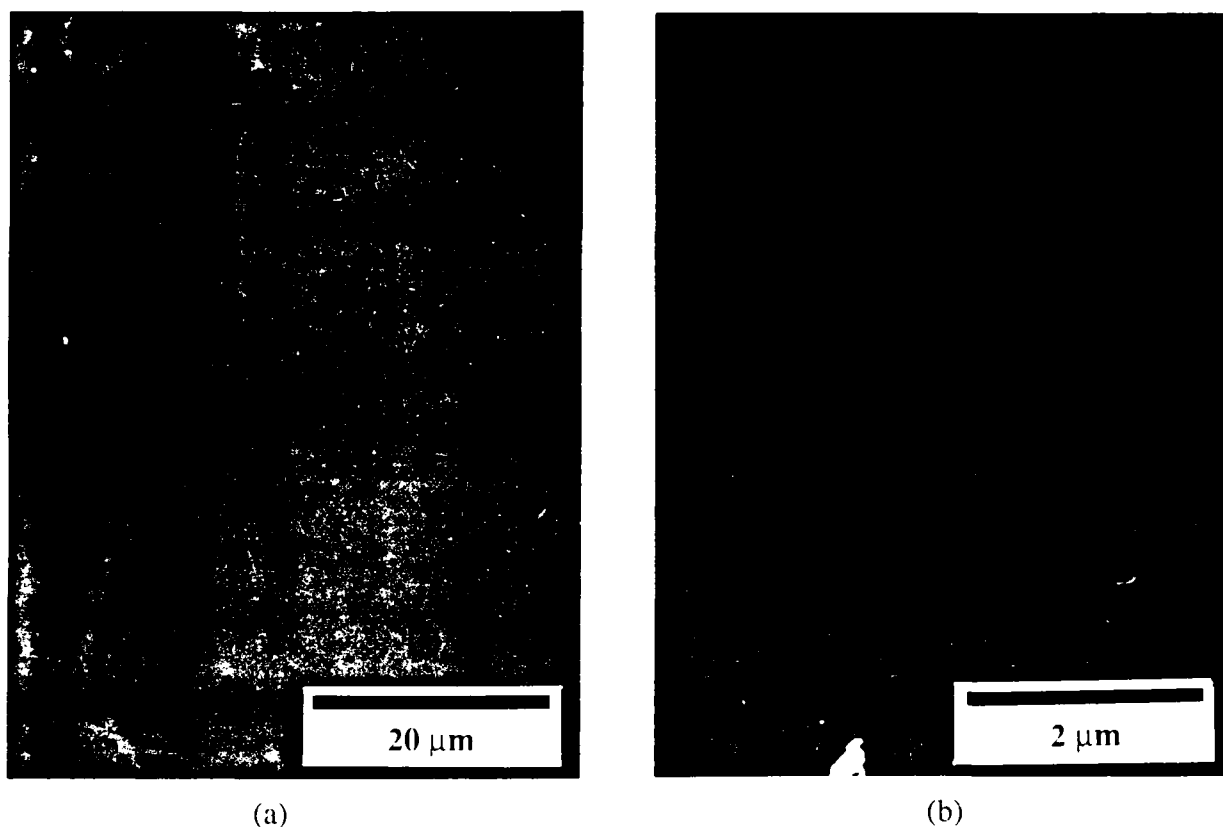


Figure 17. High resolution SEM photograph of Cu (110) surface: (a) low magnification image with gray pattern of low levels of hydrocarbon contamination but smooth surface, and (b) higher magnification showing very fine texturing of surface.

BN on Copper Substrates. After deposition of the BN films, the samples were reanalyzed by XPS and LEED to determine their purity and surface structure. Figure 18 shows the XPS results for the BN on Cu (110). Note that there is no contamination apparent and that the copper peaks are quite strong. Standard sensitivity factors[47] show that copper is not present in the ratio that appears in the figure. While these sensitivity factors do not necessarily apply for the spectrometer used, the sensitivities would not likely vary dramatically.

RHEED performed after the growth showed a diffuse Cu (110) pattern indicating crystalline growth. LEED results after deposition showed that the reconstruction spots had disappeared but the basic [110] pattern remained as can be seen in Figure 19. The pattern also has a much higher background intensity than before deposition.

At higher beam energies, streaking in the  $[1\bar{1}0]$  direction is apparent as shown in Figure 20. This streaking indicates formation of small facets or steps [34].

After removal from the chamber, sample surfaces were again observed in a high resolution field emission SEM. The BN surface is shown in Figure 21.

Samples were also examined with Raman spectroscopy (in the laboratory of Robert Nemanich). There were no observable peaks in the spectra, *i.e.*, no peaks from either hexagonal or cubic phases of boron nitride.

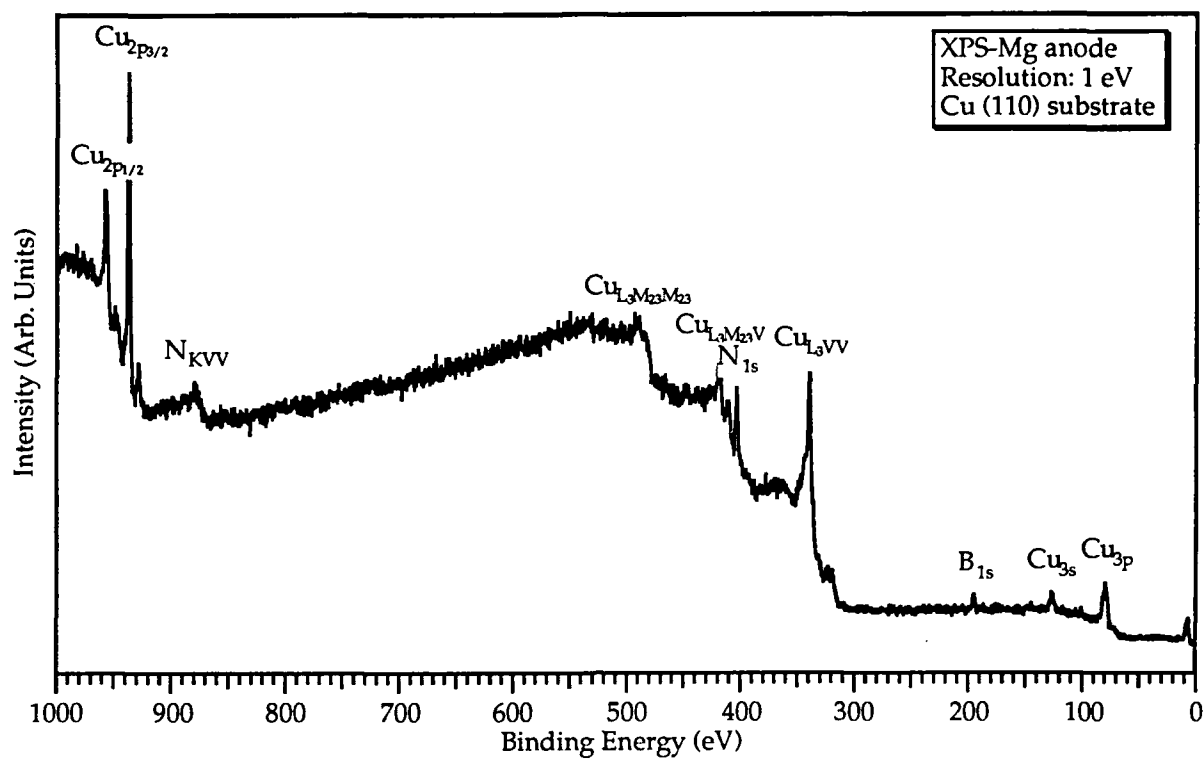


Figure 18. XPS spectrum of BN deposit on Cu(110) substrate. Cu-2p<sub>3/2</sub> sensitivity is ~50× greater than that of B-1s and ~10× greater than N-1s.



Figure 19. LEED patterns observed on BN deposited on a Cu (110) substrate showing basic (110) pattern (Beam=95.0 V).



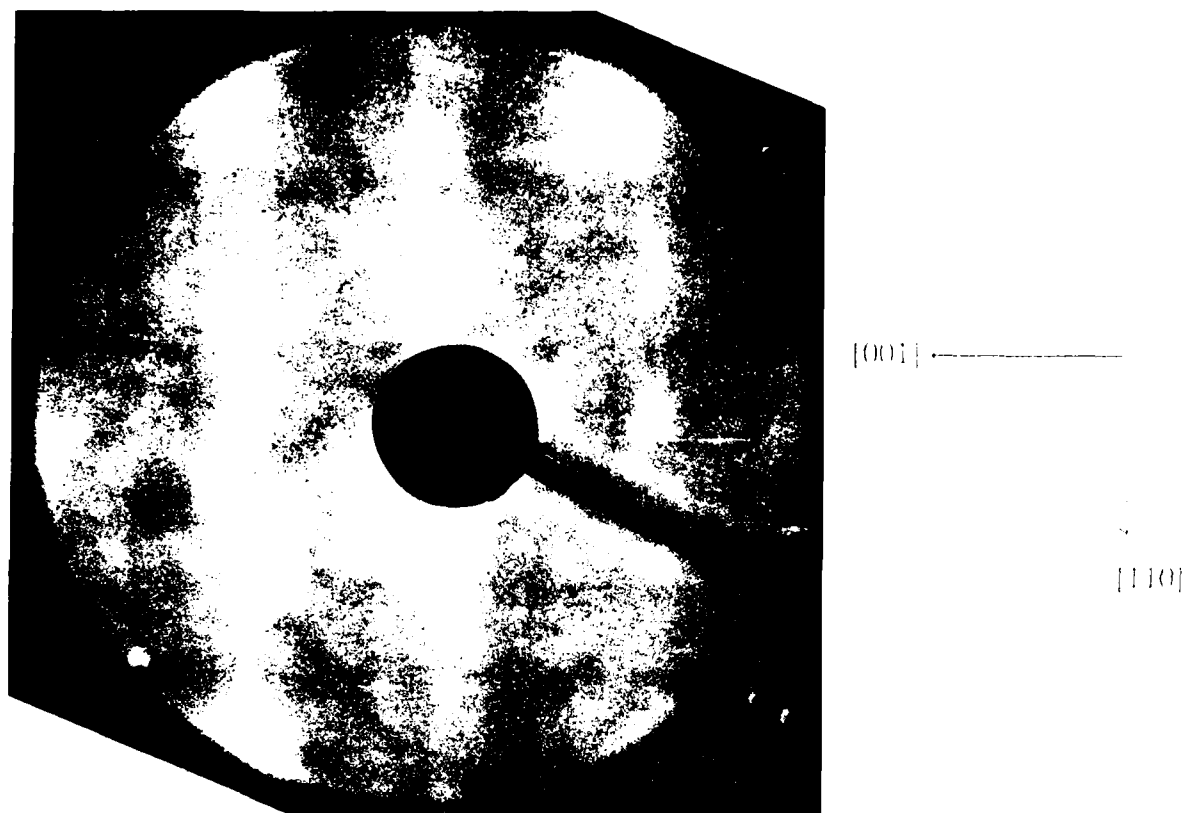


Figure 20. LEED patterns observed on BN deposited on a Cu (110) substrate showing  $(1 \times 1)$  pattern with streaks in the  $[110]$  direction (Beam=155.7 V).

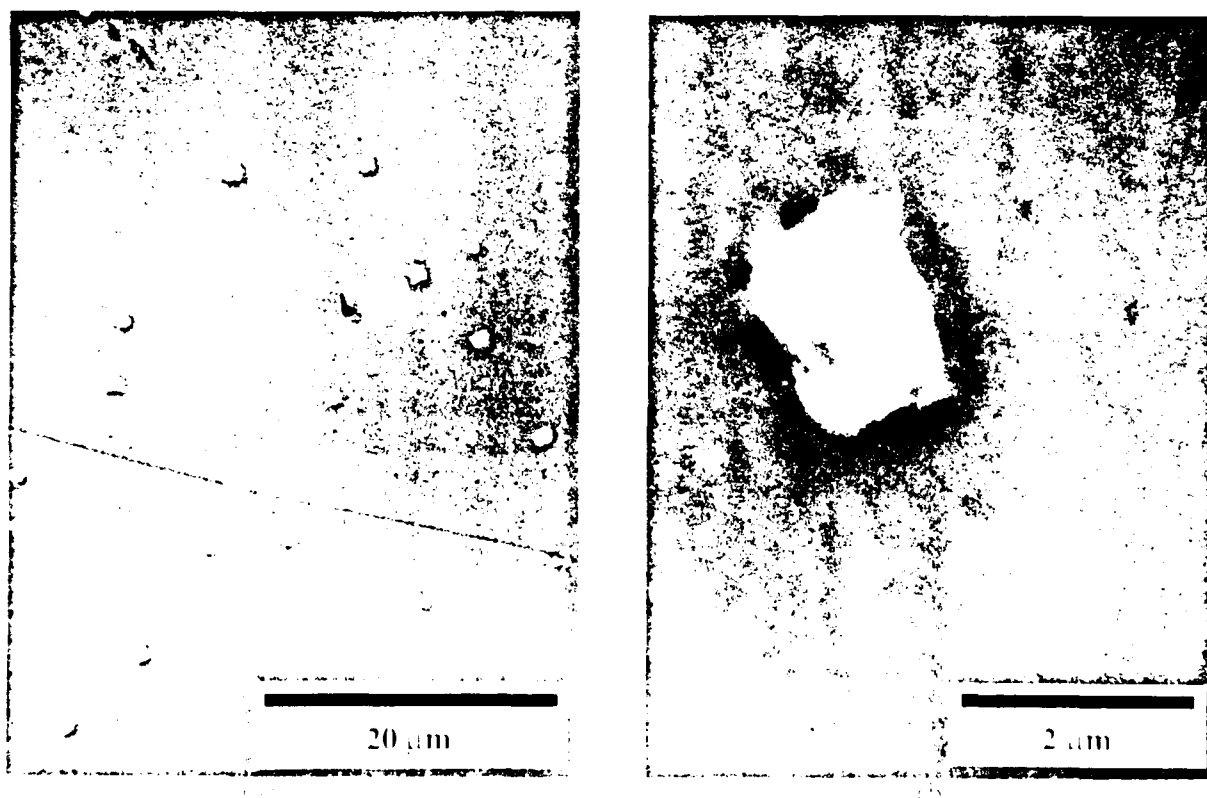


Figure 21. High resolution SEM photograph of BN on Cu (110): (a) low magnification image showing strong segregation leading to island formation, and (b) high magnification image showing structure of an individual BN island.

*Microwave Plasma CVD.* After removal from the system the films were analyzed using a rotating polarizer type ellipsometer. This gave index of refraction results for the grown films and the resulting index varied over the range of 1.65–2.28 (c-BN  $n=2.12$ ) An x-ray spectrum is shown in Figure 22, where the measured index was 2.01.

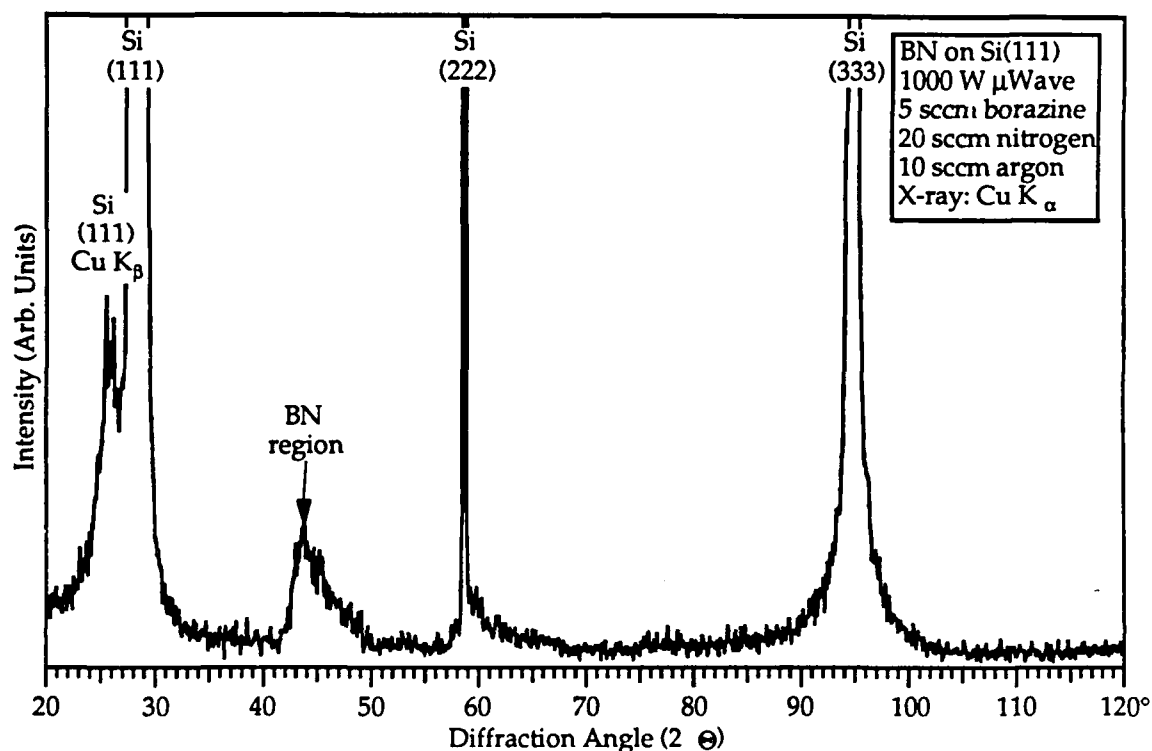


Figure 22. Typical x-ray spectrum from BN deposited in ASTeX microwave CVD system. Note BN region which cannot be resolved into individual peaks present.

FT-IR spectra of this film shows both hexagonal and cubic BN phases present along with very minor amounts of hydrogen incorporation under some processing conditions as is shown in Figures 23 and 24.

Compare that spectrum with Figure 24 which shows spectra from several different deposition conditions. Note the variation in intensity of the N-H stretch and  $3240\text{ cm}^{-1}$  peaks as well as both peaks for h-BN.

As a companion technique to the FT-IR, samples were analyzed with Raman spectroscopy. Figure 25 shows a spectrum from the best conditions film showing a mix of phases.

Next cross-section TEM samples of the apparent best condition (1000 W, 10 sccm Ar, 0 V bias) were prepared using standard techniques.[48] Shown in Figure 26 is a bright field image ( $z=[110]$ ) of the BN film with the SAD pattern in the inset. Not shown in this figure,

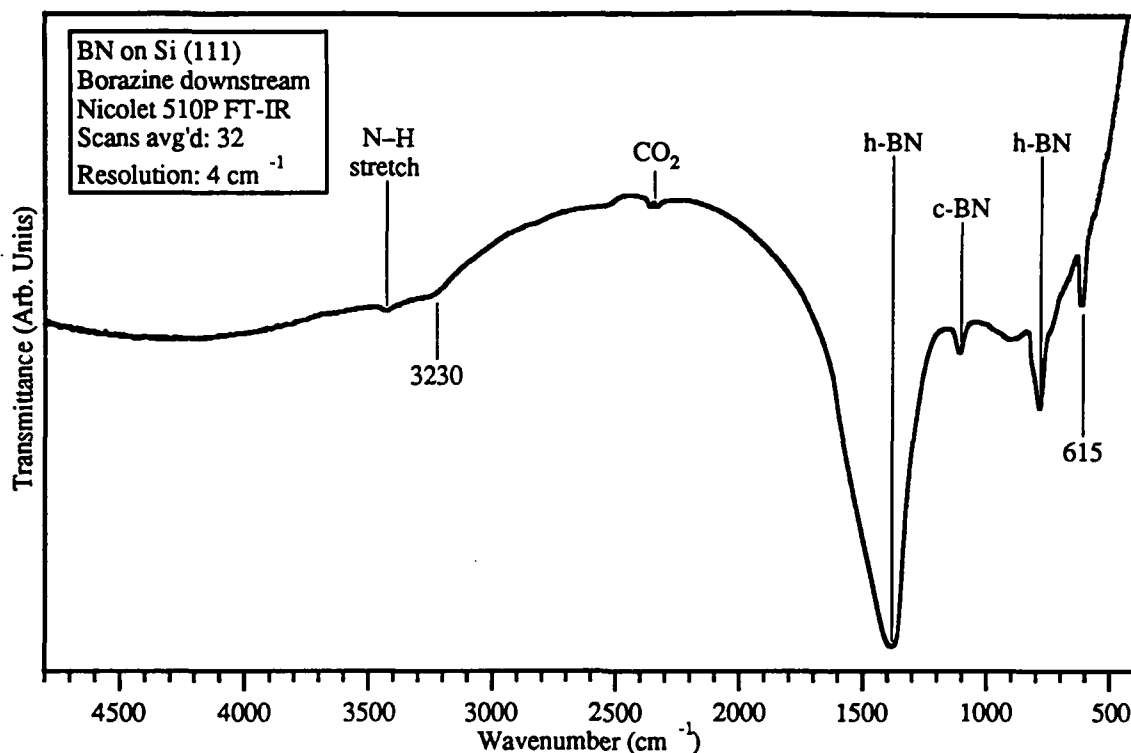


Figure 23. FT-IR spectra of BN on Si(111) showing h-BN and c-BN peaks and very little hydrogen/argon incorporation (Ar flow= 10 sccm, 1000 W, 0 V bias).

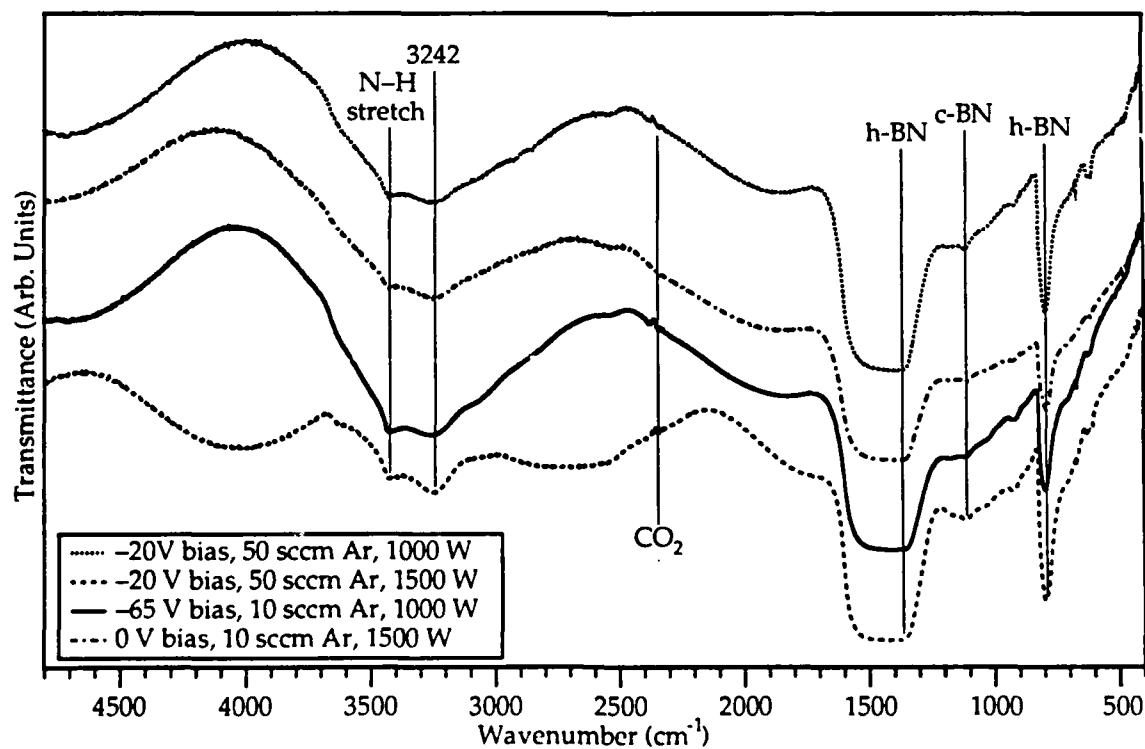


Figure 24. FT-IR spectra of BN on Si (111) under various processing conditions showing heavily distorted h-BN and c-BN (almost invisible) peaks and showing strong hydrogen/argon incorporation.

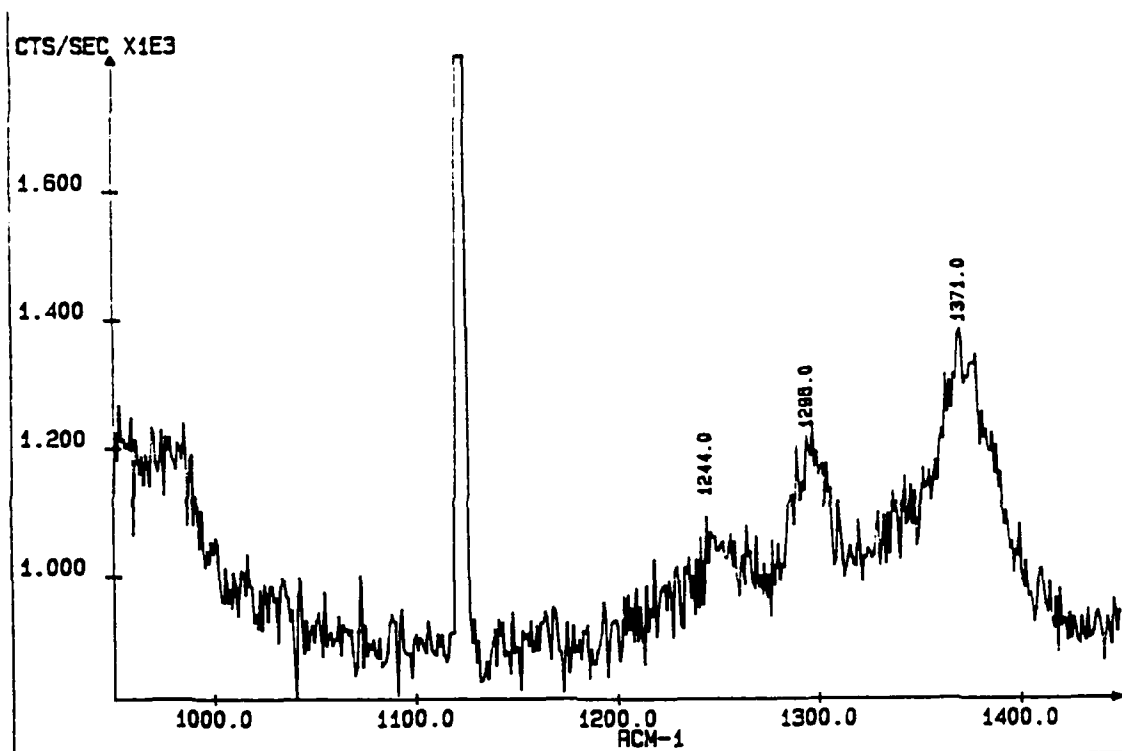


Figure 25. Raman spectrum of BN on Si (111). Shows presence of peak from h-BN ( $1371\text{cm}^{-1}$ ), c-BN ( $1295\text{ cm}^{-1}$ ), and unknown peak ( $1244\text{ cm}^{-1}$ ). The offscale peak at  $\approx 1120\text{ cm}^{-1}$  is due to overhead lights and should be ignored.

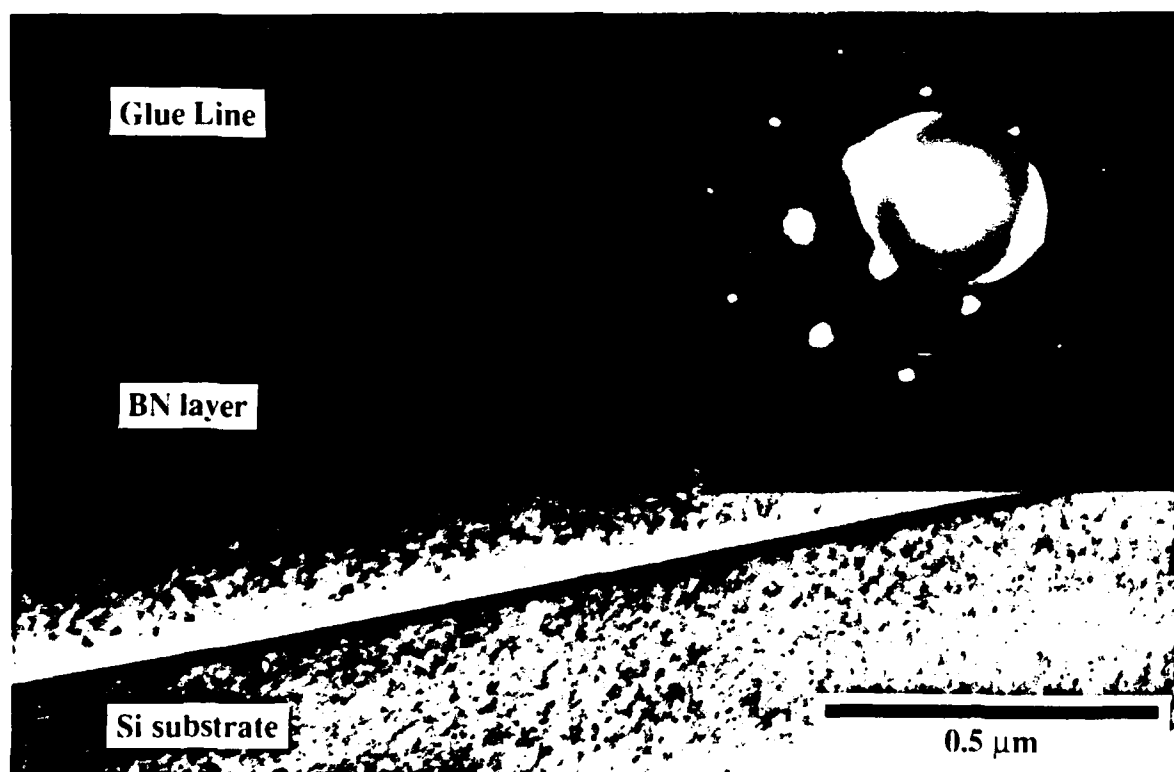


Figure 26. XTEM photograph of BN on Si (111) with  $z=[110]$ . Inset shows SAD pattern of Si with oriented polycrystalline h-BN.

but observed were areas of amorphous nature as well. The film is measured to be  $0.7\text{ }\mu\text{m}$  thick which corresponds to a  $1.4\text{ }\mu\text{m/hr}$  growth rate.

Samples grown at high substrate bias condition ( $\geq 50\text{ V}$ ) delaminated from the Si substrate. Pieces of the delaminated films were placed on nickel grids and examined in the TEM. Figure 27 shows an SAD patterns from a typical region of the BN layer.



Figure 27. SAD pattern typical of BN layers showing diffuse rings indicative of amorphous nature with some sharper rings showing hexagonal structure.

#### E. Discussion

##### *Gas Source MBE*

*BN on Silicon (100) Substrates.* The FT-IR spectra shown in Figure 13 indicates the presence of a-BN and c-BN. The peaks labeled a-BN are in the same location as seen for h-BN. This points to a minor problem in that the infrared absorption spectra cannot seemingly differentiate between amorphous BN (a-BN) and h-BN. For example, Ikeda *et al*[24] reported IR peaks for a-BN in the same location as they occur for h-BN.[49] This is because while the c-BN peak is due to a three dimensional process (transverse optical or TO) phonon while the h-BN peaks are due to B-N stretching and B-N-B bending, which are lower-dimensional processes. We suggest that these lower-dimensional processes are perhaps not sufficiently sensitive to long range order to differentiate between amorphous and hexagonal phases. Thus

the assignment of these peaks as a-BN rather than h-BN is based on x-ray and TEM diffraction data as well, and not just FT-IR information alone.

Copper Substrates. The initial state of the growth state is important to the formation of high quality deposited films. It may be even more critical in the case of c-BN, as the cubic periodicity of the substrate surface may help induce the metastable formation of c-BN.

The initial substrates were found to have significant levels sulfur contamination as was shown in Figure 14. The source of sulfur is unclear at present, but a common electrochemical etching solution (used after mechanical polishing) is mercapto-sulfur based,[46] and thus is a likely candidate source of the sulfur. This sulfur would most likely appear as  $\text{Cu}_2\text{S}$  (m.p.  $\approx 1100^\circ\text{C}$ ), since sulfur has a low boiling point ( $\approx 450^\circ\text{C}$ ) and would have been removed by the anneal. The split peak in the sulfur Auger spectrum of Figure 14 may indicate presence two types of sulfide, but by itself, is not sufficient evidence to determine the states of sulfur on the copper surface.

Clean Cu (110) surfaces have a simple  $(1\times 1)$  structure,[20] whereas sulfur adsorbed on Cu (110) induces several different surface reconstructions, depending on the amount of coverage. Boulliard and Sotto[50] reported that Domange had determined the saturation coverage of sulfur on Cu (110) to be 0.64. Boulliard and Sotto found that sulfur induced numerous reconstructions changing with increasing normalized fraction of the saturation level ( $\theta$ ). At near saturation levels ( $0.7 \leq \theta \leq 1.0$ ), they observed  $(1/2, 1/2)$  doublets in the  $[1\bar{1}0]$  direction. They also observed as coverage increased, the separation of the doublets increased until it became a  $c(8\times 2)$  structure. They also mention that at or near saturation, others observed a  $c(2\times 3)$  structure.

Figures 15 and 16 together show indications of the widely separated  $(1/2, 1/2)$  doublets in the  $[1\bar{1}0]$  direction, indicating a near saturation coverage of sulfur. In addition the spots are diffuse which may indicate disorder in the sulfur surface, which may explain the splitting observed in the sulfur Auger peak.

It has been reported by Yarmoff and Williams[51] that a LEED pattern with small spot size and low background intensity does not necessarily reflect a well-ordered surface in copper. However, their annealing steps were at a homologous temperature of only  $0.43 T_m$ , while these substrates were annealed at  $0.59 T_m$ . So it is expected that the copper near-surface region is at the very least, approaching a well-ordered condition and the diffuse spots are from disorder in the sulfur coverage, rather than disorder in the underlying copper lattice.

BN on Copper Substrates. The XPS spectrum in Figure 18 showed that that the sulfur and trace carbon are now completely gone and only copper, boron, and nitrogen remain. Note that the copper was still very much in evidence after deposition of a film which should have been  $\sim 500 \text{ \AA}$  thick. Given the surface sensitivity of the technique, this thickness would very

thoroughly eliminate the copper peaks from the spectrum. The large difference in elemental sensitivities shows that the substrate is covered more completely than it first appears, but does not explain why the copper peaks are still present.

This is most likely due to island formation which occurs when the surface energy of the adlayer is higher than that of the substrate. As was discussed in the Introduction, the surface energy of c-BN is over four times as much as that of copper (1430 vs. 4770 erg/cm<sup>2</sup>). [14, 31] This large difference is a strong driving force for the formation of islands on the surface rather than the smooth film desired. Island formation is also indicated by the LEED photographs shown in Figures 19 and 20. The basic Cu (110) pattern is still evident in Figure 19 though more diffuse and Figure 20 shows that the [1 $\bar{1}$ 0] spot splitting has become simple streaking along the same direction. These streaks are usually attributed to formation of directional steps or facets along the surface.

The idea of island formation is confirmed after examination of the surface with a high resolution SEM as was shown in Figure 21(a) and (b). Islands are clearly visible in both micrographs with a rectangular structure evident in Figure 21(b). The Raman spectra from these samples gave no evidence of either cubic or hexagonal structure. This may be due to being amorphous or to being microcrystalline as Ikeda *et al* have attributed to their films. [27] It should be emphasized that due to the strong island formation observed, that the RHEED and LEED results cannot be used as indicator as to the crystalline nature of the BN deposit, and will thus require further analysis to determine the structure.

*Microwave Plasma CVD.* The x-ray diffraction spectrum in Figure 22 shows only a broad band of reflections in the region of 42–50° 2 $\theta$ , which as can be seen from Table III covers a number of peaks from all phases of BN. The Si (111) Cu K $\beta$  peak is exactly where predicted, but is somewhat unlikely since the detector has a graphite monochromator to reduce that peak. The h-BN (002) peak is either obscured in the lower edge of Si (111) peak, or has shifted down slightly and is where the Cu K $\beta$  peak should be. If this were the case, its relative intensity would seem to indicate a significant portion of the broad BN region is from phases other than h-BN. The fact that the region is continuous also indicates at least some amorphous component.

The FT-IR spectrum shown in Figure 23 shows a fairly clean spectrum with only very slight hydrogen/argon incorporation as indicated by the almost undetectable peaks in the 3200–3500 cm<sup>-1</sup> range. The peak at 615 cm<sup>-1</sup> has not been identified and only occurred in this spectrum while the peak at 3230 cm<sup>-1</sup> is apparently related to incorporation as will be discussed next.

Table III. Diffraction peaks for phases of BN using Cu K $\alpha$  radiation.  
(Source: JCPDS card file on CD-ROM)

Crystal Phase	Relative Intensity	Crystal Plane	Diffraction Angle
h-BN	100	002	26.8°
w-BN	100	100	40.8°
h-BN	15	100	41.6°
w-BN	70	002	42.7°
c-BN	100	111	43.3°
h-BN	6	101	43.9°
w-BN	45	101	46.3°
h-BN	9	102	50.1°
c-BN	5	200	50.4°
h-BN	6	004	55.2°
h-BN	<1	103	59.6°
w-BN	18	102	60.6°
w-BN	45	101	46.3°
h-BN	9	102	50.1°
c-BN	5	200	50.4°
h-BN	6	004	55.2°
h-BN	<1	103	59.6°
w-BN	18	102	60.5°
h-BN	2	104	71.4°
c-BN	24	220	74.1°
w-BN	25	110	74.2°
h-BN	5	110	75.9°
w-BN	16	103	80.8°
h-BN	5	112	82.2°
h-BN	<1	105	85.5°
h-BN	<1	006	87.9°
w-BN	12	112	89.6°
c-BN	8	311	89.9°
h-BN	<1	200	90.5°
h-BN	1	202	96.7°
h-BN	3	114	100.7°
h-BN	<1	106	102.5°
w-BN	<1	202	103.6°
h-BN	<1	204	115.9°
c-BN	2	400	116.9°
w-BN	<1	203	124.6°
w-BN	<1		133.0°
h-BN	<1	008	135.6°
h-BN	1	116	136.1°
c-BN	3	331	136.4°
h-BN	<1	210	140.0°
h-BN	<1	212	150.8°

The spectra in Figure 24 all show strong peaks of various intensities in the 3200–3500 cm<sup>-1</sup> range and broadening of the B–N stretching mode to range from 1380–1550 cm<sup>-1</sup>.



The causes for these peaks is not understood at present but is believed to be due to a combination of incorporation of hydrogen and/or argon. It seems that any of Ar flow rates  $\geq 10$  sccm, or microwave power levels above 1000 W, or bias conditions above  $\sim 20$  V or less, that hydrogen and perhaps argon begin to be incorporated into the growing film.

Further crystal information can be seen in the Raman spectrum in Figure 25. Hexagonal BN has one Raman active peak at  $1368\text{ cm}^{-1}$  while c-BN has two peaks, the TO at  $1055\text{ cm}^{-1}$  and the LO at  $1308\text{ cm}^{-1}$ . [52] These values for BN were also confirmed by use of standards in the system used here. The h-BN peak and the LO (longitudinal optical) phonon of c-BN are clearly present, though apparently shifted slightly by stress. In addition there is another ill-defined peak which has not been identified. More importantly, this spectrum also does not show the TO phonon mode at  $1055\text{ cm}^{-1}$ , which may be due either to stress or other effects not yet determined.

TEM shown in Figures 26 and 27 show that the deposited layers are oriented h-BN. Additional areas not shown showed very diffuse rings from a-BN. This was especially true of the highest bias conditions ( $\sim 65$  V). While no c-BN was observed in the SAD patterns, this is not surprising given the polycrystalline/amorphous nature of much of the film. As can be seen from Table III, there are no c-BN planes which do not have h-BN or w-BN planes nearby, and so without larger single phase regions, c-BN would be extremely difficult to unambiguously identify.

## F. Conclusions

BN thin films were deposited on Si and Cu substrates via gas source MBE and analyzed using a variety of techniques. Resulting films appeared to be amorphous with some cubic character as determined via x-ray diffraction and noted in the previous progress report. FT-IR confirmed those results showing peaks for a-BN (as confirmed by TEM) and c-BN (not observed in TEM). Identification of c-BN phase via SAD in a fine grained mixed phase film is not possible due to the fact that diffraction peaks from c-BN are typically very close to peaks from other phases. Phase identification for Cu substrates is not complete at present, as it will require different analytical techniques to properly determine composition. Raman spectroscopy has proved ineffective in determining the composition of what is likely microcrystalline in nature. The FT-IR system is currently only configured for transmission measurements and will need to be modified to reflection mode for use on copper substrates.

BN thin films on Si via microwave plasma CVD showed a mixed composition of amorphous, hexagonal and cubic phases of BN. Evidence of hydrogen/argon incorporation was observed at high deposition power and bias levels, as well as high argon flow rates.

## G. Future Research Plans/Goals

### *Use of Copper Substrates*

Copper Cleaning. For proper use of the copper substrates, the surface will need to be made completely clean, *i.e.*, the sulfur will need to be removed. Given the thermal stability of  $\text{Cu}_2\text{S}$  ( $m.p. \approx 1100^\circ\text{C}$ ), thermal desorption is not an option and thus some sort of a chemical cleaning will be required. If wet chemical etching ( $\text{Cu}_2\text{S}$  is soluble in  $\text{HNO}_3$  and  $\text{NH}_4\text{OH}$ ) before loading into the MBE does not remove the sulfur from the copper, hydrogen plasma cleaning will be required. Dosing of  $\text{Cu}_2\text{S}$  with molecular hydrogen while heated will not reduce the  $\text{Cu}_2\text{S}$  back to Cu based on thermodynamic calculations, but dosing with atomic hydrogen will reduce the  $\text{Cu}_2\text{S}$ . [53, 54]

Boron Diffusion in Copper. Boron has a low solubility in copper ( $\approx 0.5$  at.%). If boron were diffused into copper at a high temperature and then cooled the boron would migrate to the surface. Since the boron species would migrate to sites on the copper surface, they would already possess the same symmetry as would be present in c-BN. Then bringing in atomic nitrogen from the plasma source to react with the diffusing boron, would allow the c-BN phase to form more readily, and more uniformly across the surface of the copper substrate. This would not only improve the phase stability but help to resist the driving force for island formation which is quite strong for c-BN on copper. Some boron diffusion and implantation has already taken place. Growth on these samples will be conducted momentarily.

Nitrogen as Surfactant. An additional potential advantage in use of copper substrates relates to the use of nitrogen as a surfactant in the growth of c-BN films. Surfactants have been used successfully in the system Si/Ge/Si to suppress island formation. [55] Dosing Cu with atomic N does form a  $\text{Cu}_3\text{N}$  phase, [29] which is cubic with a lattice parameter of  $3.815 \text{ \AA}$ . It is not a strongly bonded compound and decomposes at temperatures in the range of  $3\text{--}500^\circ\text{C}$ . [29, 56] There has also been reported a  $\text{Cu}_4\text{N}$  phase which is more difficult to form, but is still cubic, with a lattice parameter of  $3.193 \text{ \AA}$ , and decomposes above  $\approx 550^\circ\text{C}$ . [57]

Thus the nitride phase would form if growth temperatures were in the  $3\text{--}500^\circ\text{C}$  range, and would retain the same surface symmetry, and have a similar lattice parameter to the host Cu lattice (especially for the  $\text{Cu}_3\text{N}$  phase). This would provide an ideal surface for incoming boron atoms, since the copper nitride phase would be very unstable with respect to the formation of the c-BN, and thus an exchange reaction would be expected where boron would exchange positions with the nitrogen in forming the c-BN. This would immediately leave the c-BN with a nitrogen terminated surface, and is expected to reduce the mobility of the boron atoms and thus decrease the tendency for island formation. This approach requires lowering of growth temperatures, which has its own set of advantages and disadvantages.

### *Lowered Growth Temperatures*

*Best Observed Growth Temperatures.* A number of researchers (see references in the Introduction) have found that the best conditions for c-BN formation involve lowered growth temperatures often in the range of  $\sim 400^\circ\text{C}$ . This low growth temperature in some manner not yet understood, aids the metastable formation process required for c-BN, or at least inhibits the formation of h-BN.

However, this temperature range is extremely low for a material with as high a Debye temperature as c-BN ( $\theta_D \approx 17\text{--}1900\text{K}$ ). [14] This low temperature growth greatly inhibits surface mobility and would be expected to lead to a large amorphous component of the film, as was observed in this study. Thus, an important part of this lowered growth temperature process must be providing a source of additional energy for surface mobility to aid the crystallization process. This energy is provided in part by metastable species coming from the plasma source. However, bias is often required in addition, and the high energy bombardment caused by this bias will cause formation of many crystal defects. An alternative to substrate bias would be preferred and could take the form of ultraviolet (UV) irradiation.

*Ultraviolet Irradiation.* UV irradiation can enhance many different processes associated with the growth process. Boron has strong spectral lines at  $\approx 2497 \text{ \AA}$ , and so UV radiation could be used to create excited boron atoms which would give it a additional energy state roughly equivalent to the energy it would attain upon condensation on the growth surface. Using models of tungsten condensation on tungsten, [58] this would provide one or more surface hops to find the optimum position. Addition of just one hop, enhances the density of the film.

*Laser Ablation.* As was discussed in the last report, Doll *et al* [28, 59] has reported the successful growth of c-BN on Si by laser ablation using a KrF excimer laser. Some experiments were undertaken last fall in an attempt to reproduce this work, but resulted in understoichiometric, mixed phase deposits that did not include c-BN. It was thought that part of the problem was low laser fluences with respect to those used by Doll *et al*. A new laser has since been put in place, with much higher fluences, and it is hoped that new experiments can proceed to reproduce the results of Doll *et al*.

### H. Acknowledgements

The microwave plasma CVD work conducted at ASTeX, Inc. was funded by ASTeX, Inc.

### III. References

1. T. Suntola and J. Atson, U.S. Patent 4 058 430, Nov. 15 (1977).
2. C. H. L. Goodman and M.V. Pessa, J. Appl. Phys. **60**, R65 (1986).
3. S. M. Bedair, M. A. Tischler, T. Katsuyama and N.A. El-Masry, Appl. Phys. Lett. **47**, 51 (1985).

4. J. Nishizawa, H. Abe and T. Kurabayashi, *J. Electrochem. Soc.* **132**, 1197 (1985).
5. R. C. Weast ed., *Handbook of Chemistry and Physics*, 69<sup>th</sup> Edition 1988-1989, CRC Preess, Inc., Boca Raton, Florida.
6. L. Pauling, *The Chemical Bond*, Cornell University Press, N.Y., 1967.
7. V. I. Vedeneev, *Bond Energies, Ionization Potentials and Electron Affinities*, St Martin's Press, N.Y., 1966.
8. T. L. Cottrell, *The Strengths of Chemical Bonds*, Butterworths Scientific Publications, London, UK, 1954.
9. C. P. Foley and J. Lyngdal, *J. Vac. Sci. Technol. A* **5**, 1708 (1987).
10. R. H. Wentorf Jr., *J. Chem. Phys.* **36**, 1990 (1962).
11. R. M. Chrenko, *Solid State Commun.* **14**, 511 (1974).
12. C. Deshpandey and R. F. Bunshah, *Thin Solid Films* **163**, 131 (1988).
13. N. Miyata, K. Moriki, and O. Mishima, *Phys. Rev. B* **40**(17), 12028 (1989).
14. R. C. DeVries, *Cubic Boron Nitride: Handbook of Properties*, Technical Information Series, General Electric Company, Corporate Research and Development, 72CRD178, 1972.
15. K. H. Seidel, K. Reichelt, W. Schaal, and H. Dimigen, *Thin Solid Films* **151**(2), 243 (1987).
16. M. Mieno and T. Yoshida, *Jpn. J. Appl. Phys.* **29**(7), 1175 (1990).
17. M. Satou and F. Fujimoto, *Jpn. J. Appl. Phys.* **22**(3), L171 (1983).
18. Y. Andoh, *et al.*, *Nucl. Instrum. Meth. Phys. Res. B* **19/20**, 787 (1987).
19. J. Kouvetakis, V. V. Patel, C. W. Miller, and D. B. Beach, *J. Vac. Sci. Technol. A* **8**(6), 3929 (1990).
20. H. Saitoh, T. Hirose, H. Matsui, Y. Hirotsu, and Y. Ichinose, *Surf. Coat. Technol.* **39-40**(1-3), 265 (1989).
21. M. Okamoto, H. Yokoyama, and Y. Osaka, *Jpn. J. Appl. Phys.* **29**(5), 930 (1990).
22. A. Chayahara, H. Yokoyama, T. Imura, and Y. Osaka, *Appl. Surf. Sci.* **33/34**, 561 (1988).
23. O. Matsumoto, M. Sasaki, H. Suzuki, H. Seshimo, and H. Uyama, in *Tenth International Conference on Chemical Vapor Deposition*. G. W. Cullen, Ed. (The Electrochemical Society, Honolulu, Hawaii, 1987), pp. 552.
24. T. Ikeda, Y. Kawate, and Y. Hirai, *Kobelco Technol. Rev.* **6**, 1 (1989).
25. M. Murakawa and S. Watanabe, *Surf. Coatings Technol.* **43/44**(1-3), 128 (1990).
26. T. Nagatomo, Y. Hatooka, and O. Omoto, *Trans. IECE Jpn. E* **69**(4), 482 (1986).
27. T. Ikeda, Y. Kawate, and Y. Hirai, *J. Vac. Sci. Technol. A* **8**(4), 3168 (1990).
28. G. L. Doll, J. A. Sell, L. Salamanca-Riba, and A. K. Ballal, in *Spring 1990 Meeting of the Materials Research Society*. J. T. Glass, Eds. Boston, MA, 1990 (in press).
29. D. Heskett, A. Baddorf, and E. W. Plummer, *Surf. Sci.* **195**(1-2), 94 (1988).
30. V. R. Juza and H. Hahn, JCPDS Card #2-1156, Powder Diffraction File, JCPDS, 2-1156, 1938.
31. C. R. Barrett, W. D. Nix, and A. S. Tetelman, *The Principles of Engineering Materials* (Prentice-Hall, Inc., Englewood Cliffs, New Jersey, 1973).
32. Z. Sitar, M. J. Paisley, D. K. Smith, and R. F. Davis, *Rev. Sci. Instrum.* **61**(9), 2407 (1990).
33. J. E. Mahan, K. M. Geib, G. Y. Robinson, and R. G. Long, *J. Vac. Sci. Technol. A* **8**(5), 3692 (1990).
34. L. J. Clarke, *Surface Crystallography: An Introduction to Low Energy Electron Diffraction* (John Wiley & Sons, New York, 1985).
35. G. M. Ingo, N. Zacchetti, D. della Sala, and C. Coluzza, *J. Vac. Sci. Technol. A* **7**(5), 3048 (1989).

36. R. Trehan, Y. Lifshitz, and J. W. Rabalais, *J. Vac. Sci. Technol. A* **8**(6), 4026 (1990).
37. K. Nakamoto, *Infrared and Raman Spectra of Inorganic and Coordination Compounds* (John Wiley and Sons, New York, 1986).
38. G. Turrell, *Infrared and Raman Spectra of Crystals* (Academic Press, New York, 1972).
39. T. Yogo and S. Naka, *J. Mater. Sci.* **25**(1a), 374 (1990).
40. T. K. Paul, P. Bhattacharya, and D. N. Bose, *Appl. Phys. Lett.* **56**(26), 2648 (1990).
41. W. L. Lin, Z. Xia, Y. L. Liu, and Y. C. Fen, *Mater. Sci. Eng. B* **B7**(1), 107 (1990).
42. S. Y. Shapoval, *et al.*, *Appl. Phys. Lett.* **57**(18), 1885 (1990).
43. M. Yoshikawa, *et al.*, *Appl. Phys. Lett.* **57**(5), 428 (1990).
44. J. R. Vig, *J. Vac. Sci. Technol. A* **3**(3), 1027 (1985).
45. H. Lamb, NCSU, personal communication, 1990.
46. I. Villegas, C. B. Ehlers, and J. L. Stickney, *J. Electrochem. Soc.* **137**(10), 3143 (1990).
47. C. D. Wagner, W. M. Riggs, L. E. Davis, and J. F. Moulder, *Handbook of X-ray Photoelectron Spectroscopy* (Perkin-Elmer Corporation, Eden Prairie, MN, 1979).
48. J. C. Bravman and R. Sinclair, *J. Electron Microsc. Techniq.* **1**, 53 (1984).
49. R. Geick, C. H. Perry, and G. Rupprecht, *Phys. Rev.* **146**(2), 543 (1966).
50. J. C. Boulliard and M. P. Sotto, *Surf. Sci.* **217**, 38 (1989).
51. J. A. Yarmoff and R. S. Williams, *Surf. Sci.* **165**(2-3), L73 (1986).
52. D. R. Clarke and F. Adar, in *Advances in Materials Characterization*. D. R. Rossington, R. A. Condrate, and R. L. Snyder, Eds. (Plenum Press, Alfred University, 1982), pp. 199.
53. M. W. Chase Jr., *et al.*, *JANAF Thermochemical Tables* (American Chemical Society, Midland, MI, 1985).
54. O. Kubaschewski and C. B. Alcock, *Metallurgical Thermochemistry* (Pergamon Press Ltd., New York, 1979).
55. M. Copel, M. C. Reuter, E. Kaxiras, and R. M. Trump, *Phys. Rev. Lett.* **63**(6), 632 (1989).
56. M. Asano, K. Umeda, and A. Tasaki, *Jpn. J. Appl. Phys.* **29**(10), 1985 (1990).
57. J. Blucher, K. Bang, and B. C. Giessen, *Mater. Sci. Eng. A* **117**, L1 (1989).
58. R. D. Young and D. C. Schubert, *J. Chem. Phys.* **42**(11), 3943 (1965).
59. G. L. Doll, J. A. Sell, C. A. Taylor II, and R. Clarke, *Phys. Rev. B* **43**(8), 6816 (1991).